

# REPORT DOCUMENTATION PAGE

Form Approved  
OMB No. 0704-0188

Public reporting burden for this collection of information is estimated to average 1 hour per response, including the time for reviewing instructions, searching existing data sources, gathering and maintaining the data needed, and completing and reviewing this collection of information. Send comments regarding this burden estimate or any other aspect of this collection of information, including suggestions for reducing this burden to Department of Defense, Washington Headquarters Services, Directorate for Information Operations and Reports (0704-0188), 1215 Jefferson Davis Highway, Suite 1204, Arlington, VA 22202-4302. Respondents should be aware that notwithstanding any other provision of law, no person shall be subject to any penalty for failing to comply with a collection of information if it does not display a currently valid OMB control number. **PLEASE DO NOT RETURN YOUR FORM TO THE ABOVE ADDRESS.**

<b>1. REPORT DATE (DD-MM-YYYY)</b> June 2004		<b>2. REPORT TYPE</b> Journal Article		<b>3. DATES COVERED (From - To)</b> 2004	
<b>4. TITLE AND SUBTITLE</b>  Pseudoelastic SMA Spring Elements for Passive Vibration Isolation: Part I - Modeling				<b>5a. CONTRACT NUMBER</b>	
				<b>5b. GRANT NUMBER</b>	
				<b>5c. PROGRAM ELEMENT NUMBER</b>	
<b>6. AUTHOR(S)</b>  Mughees M. Khan, Dimitris C. Lagoudas, John J. Mayes,* and Benjamin K. Henderson**				<b>5d. PROJECT NUMBER</b>	
				<b>5e. TASK NUMBER</b>	
				<b>5f. WORK UNIT NUMBER</b>	
<b>7. PERFORMING ORGANIZATION NAME(S) AND ADDRESS(ES)</b>  Department of Aerospace Engineering Texas A&M University College Station, TX 77843  *V-22 Structure and Development Airframe Systems Bell Helicopter, Textron Fort Worth, TX 76101				<b>8. PERFORMING ORGANIZATION REPORT NUMBER</b>	
<b>9. SPONSORING / MONITORING AGENCY NAME(S) AND ADDRESS(ES)</b> **AFRL/VSSV 3550 Aberdeen Ave SE Kirtland AFB, NM 87117-5776				<b>10. SPONSOR/MONITOR'S ACRONYM(S)</b>	
				<b>11. SPONSOR/MONITOR'S REPORT NUMBER(S)</b>	
<b>12. DISTRIBUTION / AVAILABILITY STATEMENT</b>  Approved for public release; distribution is unlimited.					
<b>13. SUPPLEMENTARY NOTES</b> Journal of Intelligent Material Systems and Structures, Vol. 15—June 2004, pp. 415-441.					
<b>14. ABSTRACT</b> In this work, the effect of pseudoelastic response of shape memory alloys (SMAs) on passive vibration isolation has been investigated. This study has been conducted by developing, modeling, and experimentally validating a SMA-based vibration isolation device. This device consists of layers of prestrained SMA tubes undergoing pseudoelastic transformations under transverse dynamic loading. These SMA tubes are referred to as SMA spring elements in this study. To accurately model the nonlinear hysteretic response of SMA tubes present in this device, at first a Preisach model (an empirical model based on system identification) has been adapted to represent the structural response of a single SMA tube. The modified Preisach model has then been utilized to model the SMA-based vibration isolation device. Since this device also represents a nonlinear hysteretic dynamical system, a physically based simplified SMA model suitable for performing extensive parametric studies on such dynamical systems has also been developed. Both the simplified SMA model and the Preisach model have been used to perform experimental correlations with the results obtained from actual testing of the device. Based on the studies conducted, it has been shown that SMA-based vibration isolation devices can overcome performance trade-offs inherent in typical softening spring-damper vibration isolation systems. This work is presented as a two-part paper. Part I of this study presents the modification of the Preisach model for representing SMA pseudoelastic tube response together with the implemented identification methodology. Part I also presents the development of a physically based simplified SMA model followed by model comparisons with the actual tube response. Part II covers extensive parametric study of a pseudoelastic SMA spring-mass system using both models developed in Part I. Part II also presents numerical simulations of a dynamic system based on the prototype device, results of actual testing of the device and correlations of the experimental cases with the model predictions.					
<b>15. SUBJECT TERMS</b> Shape memory alloys (SMAs), pseudoelasticity, hysteresis, Preisach, system identification, passive vibration isolation, damping, dynamic system					
<b>16. SECURITY CLASSIFICATION OF:</b>			<b>17. LIMITATION OF ABSTRACT</b>  Unlimited	<b>18. NUMBER OF PAGES</b>  28	<b>19a. NAME OF RESPONSIBLE PERSON</b> Benjamin K. Henderson
<b>a. REPORT</b> Unclassified	<b>b. ABSTRACT</b> Unclassified	<b>c. THIS PAGE</b> Unclassified			<b>19b. TELEPHONE NUMBER (include area code)</b> 505-853-6712

20050112 028

# Pseudoelastic SMA Spring Elements for Passive Vibration Isolation: Part I – Modeling

MUGHEES M. KHAN,<sup>1</sup> DIMITRIS C. LAGOUDAS,<sup>1,\*</sup> JOHN J. MAYES<sup>2</sup> AND BENJAMIN K. HENDERSON<sup>3</sup>

<sup>1</sup>Department of Aerospace Engineering, Texas A&M University, College Station, TX 77843, USA

<sup>2</sup>V-22 Structure and Development, Airframe Systems, Bell Helicopter, Textron, Fort Worth, TX 76101, USA

<sup>3</sup>Air Force Research Laboratory/VSSV, Kirtland AFB, NM 87117, USA

**ABSTRACT:** In this work, the effect of pseudoelastic response of shape memory alloys (SMAs) on passive vibration isolation has been investigated. This study has been conducted by developing, modeling, and experimentally validating a SMA-based vibration isolation device. This device consists of layers of prestrained SMA tubes undergoing pseudoelastic transformations under transverse dynamic loading. These SMA tubes are referred to as SMA spring elements in this study. To accurately model the nonlinear hysteretic response of SMA tubes present in this device, at first a Preisach model (an empirical model based on system identification) has been adapted to represent the structural response of a single SMA tube. The modified Preisach model has then been utilized to model the SMA-based vibration isolation device. Since this device also represents a nonlinear hysteretic dynamical system, a physically based simplified SMA model suitable for performing extensive parametric studies on such dynamical systems has also been developed. Both the simplified SMA model and the Preisach model have been used to perform experimental correlations with the results obtained from actual testing of the device. Based on the studies conducted, it has been shown that SMA-based vibration isolation devices can overcome performance trade-offs inherent in typical softening spring-damper vibration isolation systems. This work is presented as a two-part paper. Part I of this study presents the modification of the Preisach model for representing SMA pseudoelastic tube response together with the implemented identification methodology. Part I also presents the development of a physically based simplified SMA model followed by model comparisons with the actual tube response. Part II of this work covers extensive parametric study of a pseudoelastic SMA spring-mass system using both models developed in Part I. Part II also presents numerical simulations of a dynamic system based on the prototype device, results of actual testing of the device and correlations of the experimental cases with the model predictions.

**Key Words:** shape memory alloys (SMAs), pseudoelasticity, hysteresis, Preisach, system identification, passive vibration isolation, damping, dynamic system

DISTRIBUTION STATEMENT A  
Approved for Public Release  
Distribution Unlimited

## INTRODUCTION

THE task of damping and vibration isolation is often faced with trade-offs. The goal of vibration isolation is commonly accomplished by using an isolation system with a relatively softer stiffness (Beranek and Vér, 1992). However, for isolation of heavy loads, a small stiffness leads to large displacements. This large displacement obstacle has often been overcome by using a device having a nonlinear spring with decreasing stiffness, like a softening spring. Such a device would have a stiff initial response which becomes less stiff as the load is increased, so that the stiff region of the device's response supports the initial load and

the transmissibility is reduced by the softer stiffness of the nonlinear spring in the operating range. One of the problems encountered in vibration isolation using a nonlinear spring is its resonant behavior at low excitation frequencies due to softer stiffness in the operating range. This condition results in the necessity to add damping to the system, which has the desired effect of decreasing the resonant response but also degrades the response of the system at higher frequencies as shown by Harris (1996) and Inman (2001).

To eliminate these trade-offs one can use active materials integrated into smart structures. One such option is to use Shape Memory Alloys (SMAs) as the behavior of devices with decreasing stiffness and a damper is similar to the hysteretic load-deflection relationship exhibited by SMAs during pseudoelastic

\*Author to whom correspondence should be addressed.  
E-mail: dlagoudas@aero.tamu.edu

deformation (Wayman, 1983; Otsuka and Shimizu, 1986) as discussed later.

### Review of Pseudoelastic SMA-based Dynamic Systems for Damping and/or Vibration Isolation

The SMA pseudoelastic behavior is defined as inducing detwinned martensite ( $M$ ) from austenite ( $A$ ) by thermomechanical loading, which then reverts to austenite upon removal of the mechanical load. The presence of stress forces austenite to directly form detwinned martensite, resulting in large macroscopic strains, which can be fully recovered upon unloading to the zero-stress state, provided the temperature is kept above a certain level (Wayman, 1983; Miyazaki et al., 1997; Otsuka and Wayman, 1999). Figure 1 represents a schematic of a typical SMA phase diagram, showing the relationship between stress, temperature, and the two possible phases of the SMA. Schematic of a typical pseudoelastic loading path as discussed above is also shown. The transformation temperatures at the zero-stress state are represented as  $M^{0s}$ ,  $M^0$ ,  $A^0$ , and  $A^{0s}$  in Figure 1 representing martensitic start, martensitic finish, austenitic start, and austenitic finish temperatures. In addition to the change in material properties and large recoverable strain during pseudoelastic transformation, there is hysteresis which is an indicator of energy dissipation during the forward ( $A \rightarrow M$ ) and reverse ( $M \rightarrow A$ ) transformations (Figure 1(b)). This energy dissipation is proportional to the degree of transformation completed during a loading cycle for both complete and incomplete, or partial transformations. These partial transformations are also referred to as minor loop hysteresis cycles (Bb and Lagoudas, 1999a) and complete, or full transformations are referred to as

major loop hysteresis cycles. The energy dissipation due to hysteresis provides an opportunity for SMAs to be used as damping devices and the change in the stiffness (represented by Points 1, 2, 3, and 4 in Figure 1(b)) of the material during pseudoelastic phase transformations provide opportunities for SMAs to be used as vibration isolation devices.

The nature of the pseudoelastic effect, as discussed above and illustrated in Figure 1(b), indicates the possibility of using SMAs for vibration isolation. Utilization of SMAs for such applications requires understanding of the pseudoelastic nonlinear hysteretic response found in SMAs. Graesser and Cozzarelli (1991) introduced a model for SMA hysteretic behavior, an extension of the rate independent hysteresis model introduced by Ozdemir (1976) to model pseudoelastic behavior of SMAs for potential structural damping and seismic isolation applications. A study on the use of SMAs for passive structural damping is presented in Thompson et al. (1995), where three different quasi-static models of hysteresis were reviewed and compared with an experimental investigation of a cantilevered beam constrained by two SMA wires. Fosdick and Ketema (1998), have considered rate dependency by including "averaged" thermal effects in the SMA constitutive behavior. Their constitutive model is based on dynamics of single-crystal phase boundaries by Abeyaratne and Knowles (1994), and they have studied a single degree of freedom (SDOF) lumped mass oscillator with a SMA wire attached in parallel as a passive vibration damper. Seelecke (2002), in a recent publication has considered both isothermal and nonisothermal SMA constitutive response caused by rate-dependent release and absorption of latent heat during phase transformations by using a modified

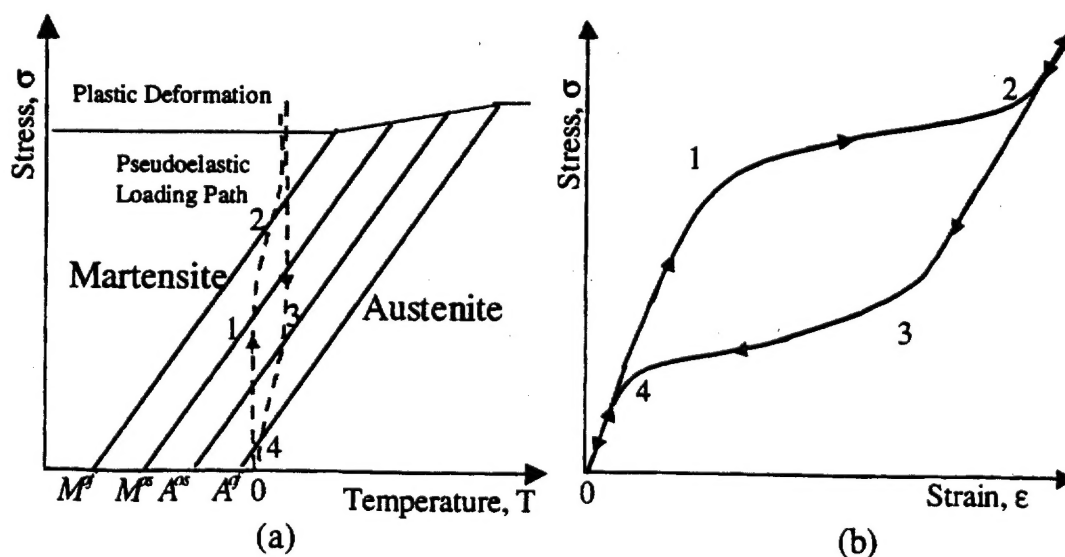


Figure 1. (a) Schematic of a typical SMA phase diagram with a typical pseudoelastic loading path noted in stress-temperature space; (b) schematic of the corresponding pseudoelastic loading path in stress-strain space.

version of the model presented by Achenbach and Muller (1985). In Seelecke (2002), free and forced vibrations of a rigid mass suspended by a thin-walled SMA tube under torsional loading has been considered under isothermal conditions. For nonisothermal conditions, only free vibrations have been considered and it has been shown that under a free vibration case for such a system, isothermal SMA constitutive response may lead to underestimation of damping and resulting forces compared to a nonisothermal SMA constitutive response.

Yiu and Regelbrugge (1995), have investigated the behavior of SMA springs designed to act as an on-orbit soft mount isolation system with the added benefit of precision alignment through the utilization of the SMA shape memory effect. Yiu and Regelbrugge (1995) have used a physically based SMA model identified from a SMA helical spring response. In the work done by Feng and Li (1996), the dynamics of a SMA bar in a SDOF spring mass damper system is presented, where the modified plasticity model presented in Graesser and Cozzarelli (1991) is used to model the pseudoelastic response of a SMA bar. Key results of this work includes that the nonlinearity due to phase transformation leads to complicated dynamics like period doubling cascade and chaotic motion. Other results include low resonant frequency for such a system along with a suppressed peak response. Experimental results have also been presented for such a system verifying qualitative predictions of the theory. A recent study by Lacarbonara et al. (2001) have studied periodic and nonperiodic thermomechanical response of a shape-memory oscillator using a modified Ivshin and Pence (1994) model and considered both isothermal and nonisothermal conditions under forced vibration and presented a rich class of solutions and bifurcations including jump phenomena, pitch fork, period doubling, complete or incomplete bubble structures with a variety of nonperiodic responses. Results presented in Lacarbonara et al. (2001) show that for the range of parameters investigated, the nonisothermal and isothermal response were similar to each other. Work presented by Lacarbonara et al. (2001) is based on an earlier work by Bernardini and Vestroni (2002), where nonlinear dynamic nonisothermal response of pseudoelastic shape memory oscillators have been presented. Softening as well as hardening behavior is noted as the SMA undergoes partial and full phase transformation under varying force excitation amplitude, hysteresis shape, and temperature. Recent work by Collet et al. (2001) have studied the behavior of a pseudoelastic SMA (Cu-Al-Be) beam under dynamic loading for potential vibration isolation applications using a SMA constitutive model presented in Ranjecki et al. (1992). Simulations and qualitative experimental observations presented in Collet et al. (2001) have shown that the

nonlinearity in the SMA beam response is due to the SMA undergoing phase transformations.

Based on the work done on SMA-based dynamic systems mentioned in the above publications there is a need to explore the effects of SMA pseudoelasticity on vibration isolation by performing actual experimental correlations and conducting parametric studies under various dynamic loading conditions on an actual SMA-based vibration isolation device. In this two-part paper series, an attempt has been made to address these issues by developing, simulating, testing, and performing parametric studies and experimental correlations on a pseudoelastic SMA vibration isolator.

### SMA Models

To realize the goal of designing and simulating an active material-based smart structure for vibration isolation using SMAs, it is necessary to have structural models that can (a) incorporate response of SMAs and (b) can be used for prediction and experimental correlation of dynamic response of such structures. Along with the SMA models mentioned in the previous section that have been mostly used for simulating SMA-based dynamic systems, most of the other SMA constitutive models available in the literature do not serve this dual purpose well. Studies of other SMA constitutive models available in the literature (Tanaka, 1986; Patoor et al., 1987; Liang and Rogers, 1990; Brinson, 1993; Lagoudas et al., 1996; Lagoudas and Bo, 1999) and their utilization for various SMA-based smart structure applications reveal that although these models are quite accurate, they are computationally intensive and/or hard to implement under dynamic loading conditions.

Empirical models based on system identification (ID) have also been used for modeling the response of different active materials and one of the most popular models has been the Preisach model. The classical Preisach model was initially proposed in the 1930s by a German physicist Preisach (1935) for ferromagnetic hysteresis effects and still is the most popular hysteresis model for ferromagnetic materials. In 1970s and 1980s, a Russian mathematician Krasnoselskii (Krasnoselskii and Pokrovskii, 1983) examined and developed the mathematical properties of the Preisach model and presented the model as a spectral decomposition of relay operators. As a result, a useful mathematical tool evolved in the form of the Preisach model which could model various hysteretic behaviors found in nature, without concern for the underlying physical mechanisms. The reader is referred to comprehensive expositions on the Preisach model by Mayergoyz (1991), Brokate (1994) and Visintin (1994) for a detailed analysis and explanation.

The generality and the computational efficiency of the Preisach hysteresis model made it applicable to the development of controller designs (Ge and Jouaneh, 1995; Hughes, 1997) and stability analysis (Gorbet et al., 1997) of hysteretic ferromagnetic, ferroelectric, and SMA actuators. Most of the work done to date on using the Preisach model has been focused toward ferromagnetic and ferroelectric materials, mainly on their application as actuators. Recently the Preisach model has been adopted for use in SMA applications. The suitability of the model for representation of SMA actuator hysteresis has been tested by Hughes (1997); Hughes and Wen (1994); Banks et al. (1996a, b, 1997) and Webb (1998) and work has progressed toward adaptive control, stability analysis, and control techniques (Gorbet et al., 1997, 1998). As the Preisach model is solely concerned with system identification and relies on additional identification experiments in case of any change in system conditions, Bo and Lagoudas (1999b) have correlated a thermomechanical model for SMA shape memory effect response with the Preisach hysteresis model to avoid the need for additional identification.

However, the above mentioned works are focused on the shape memory effect or the actuator applications of SMAs, while work done on pseudoelastic modeling of SMA hysteresis using the Preisach model is limited and only addressed in few publications. In work done by Huo (1991), the author describes a complicated extension of the Preisach model for pseudoelastic response of SMAs using a four-parameter hysteresis operator for each SMA crystal. The model is compared to experimental data for an unspecified polycrystalline material and the technique for identifying the complex model is not defined in detail and only qualitative results are given. Ortin (1992) has applied the classical Preisach model to a single crystal Cu-Zn-Al SMA which has more profound hysteresis than binary Nickel-Titanium (NiTi) SMA. Ortin's work demonstrates that the two major properties of Preisach model, the minor-loop congruency and the wipe-out property holds true for Cu-Zn-Al SMA. The control parameter was stress, the observed parameter was strain and all the tests were performed at a constant temperature. A good match has been observed between simulated output and experimental data. Song et al. (1999) have also developed a Preisach model for pseudoelastic polycrystalline Nitinol SMA wires and shown the effectiveness of modeling pseudoelastic SMA response. However, as the Preisach model is solely concerned with system identification, any change in the system conditions require additional identification. In order to correlate the model with the physical process involved in the nonlinear hysteretic behavior of SMAs and to avoid additional identification in case of any change in system conditions, Lagoudas and Bhattacharyya (1997) have

SMA response with the Preisach hysteresis model. Since a key issue for the application of the model to describe a specific material is to determine the Preisach weighting function, Lagoudas and Bhattacharyya (1997), introduced a single crystal hysteresis model, and by using appropriate averaging, estimated the weighting function or the distribution function for a polycrystalline SMA. The work presented in Lagoudas and Bhattacharyya (1997) and Bo and Lagoudas (1999b) is quite extensive. However, it leads to intensive computations, is difficult to implement and does not serve the purpose of having an accurate model suitable for design optimization analysis and simulation of dynamic systems.

In this work, a dynamic system with SMA spring components is investigated through numerical simulation and experimental correlation. This work is motivated by the need to model and experimentally validate a prototype of a SMA-based isolation system (Mayes and Lagoudas, 2001) and is a continuation of earlier works (Lagoudas et al., 2001a; Khan and Lagoudas, 2002; Lagoudas et al., 2002) presented by the authors in recent conferences. The vibration isolation device presented in this work consists of layers of prestrained SMA tubes undergoing pseudoelastic transformations under transverse dynamic loading. This study is presented as a two-part paper and Part I of this paper discusses the work done on modeling the structural pseudoelastic SMA tube response. SMA tubes are modeled and referred to as the SMA spring elements in the two-part paper. Outline of Part I is as follows: first a brief description of the vibration isolation device is presented. The experimental description is followed by an adaptation of the Preisach model (Preisach, 1935; Mayergoyz, 1991; Hughes and Wen, 1994; Ge and Jouaneh, 1995; Gorbet et al., 1998; Webb, 1998; Khan, 2002) for the structural pseudoelastic SMA tube response in order to utilize the accuracy, generality, and computational efficiency of a system ID-based model, especially for the purpose of design optimization of the prototype device and performing experimental correlations.

For the sake of quantifying effects of pseudoelasticity on a wide range of system parameters like SMA operating temperature, hysteresis, structural stiffness, hardening, softening, and displacement due to phase transformation, a computationally efficient, physically based model is also presented. This physically based SMA model is referred in the text as the simplified SMA model. Even though the simplified model is not unique in the literature and can be considered as a special case of the work done by earlier authors, its implementation in the form of this work as applied to vibration isolation has not been observed in the literature which becomes evident in Part II of this two-part study.

In this part, in addition to the modified Preisach model, the need for effective data collection for system

identification has also been presented by identifying a Preisach model from the simplified model followed by comparison of the Preisach model and the simplified model with the actual pseudoelastic SMA tube response and conclusions.

Part II of this two-part paper discusses the effect of the hysteresis and change in stiffness on a dynamic system by presenting numerical simulations of a generic pseudoelastic SMA spring mass system followed by simulations of a system based on the prototype device utilizing the models developed in Part I. Detailed description of the prototype device along with actual experimental results are also presented in Part II followed by experimental correlations of model predictions with the actual results and concluding remarks for the two-part paper series.

### BRIEF DESCRIPTION OF THE EXPERIMENTAL SETUP AND FINITE ELEMENT ANALYSIS

An experimental device was built to determine the effectiveness of SMAs when the SMA pseudoelastic response is used in a dynamic system. SMA tubes were chosen to investigate the validity of SMA spring elements as vibration isolators due to ease in manufacturing and availability of SMA tubes. In this device, layers of thin-walled SMA tubes loaded in a transverse direction in compression were used to support the mass, which was subjected to base excitations. The tubes were acquired from SMA, Inc. and were manufactured from

Nitinol with a diameter of approximately 6 mm and a wall thickness of approximately 0.17 mm. The tubes used in the experiment were cut to 10 mm in length.

A schematic of the shaker configuration with the SMA spring-mass system attached is shown in Figure 2, where SMA tubes have been shown as nonlinear springs. A typical pseudoelastic force-displacement response for a single SMA tube tested in compression at 25°C is shown in Figure 3; and as mentioned earlier, the SMA tube force-displacement response is referred to as the SMA spring force-displacement response. It should be noted that this is the structural response of a SMA tube, not the constitutive response of the SMA itself. The mechanical test for a single tube was performed on an MTS servo-hydraulic load frame with a TestStar II controller under displacement control. The SMA tube was loaded transverse to the longitudinal axis in increments up to approximately 70% reduction in diameter. Various MTS cross-head displacement loading rates were used ranging from 0.016 mm/s to 0.3 mm/s at different temperatures ranging from 25 to 65°C, all of which yielded similar force-displacement responses. The tube response showed maximum 5% of increased hardening at higher testing temperatures and all loading rates as higher stresses are required to induce the austenite to martensite phase transformation (Figure 1).

The small change in the force-displacement curves for different temperatures was attributed to the fact that only very small parts of the SMA tube were undergoing phase transformation. To validate this observation, the

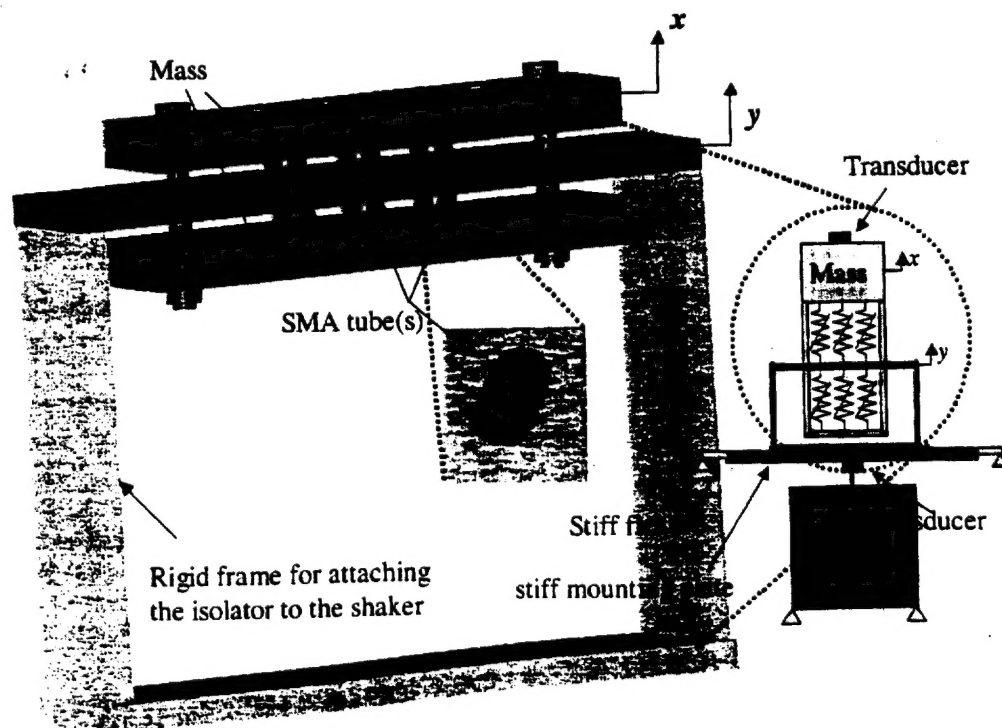


Figure 2. Schematic of shaker and SMA spring-mass isolation system as tested.

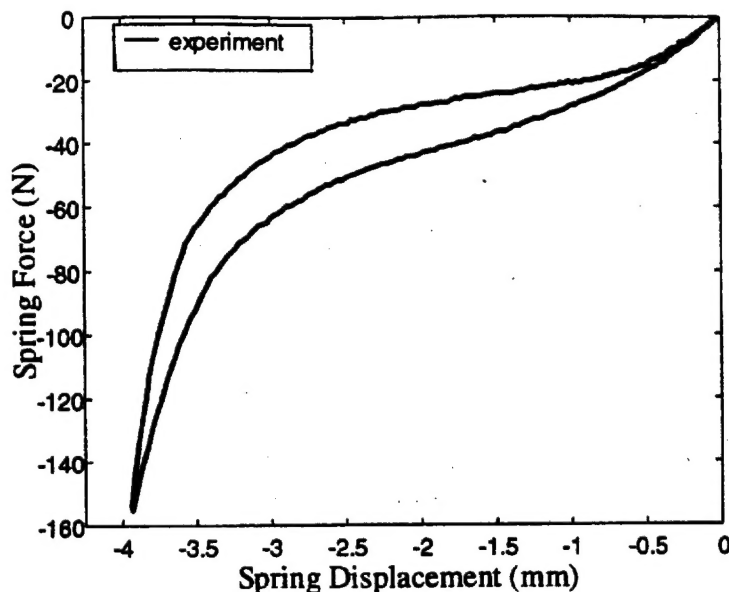


Figure 3. Pseudoelastic force-displacement response (in compression at 25°C) of a SMA tube used in the vibration isolation device.

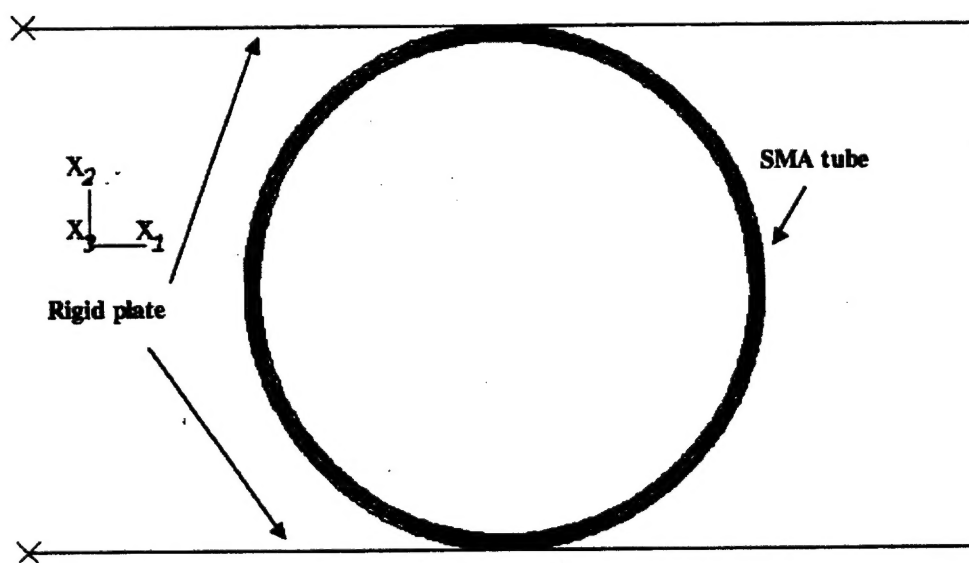


Figure 4. Finite element simulation of a SMA tube under transverse loading (undeformed configuration).

response of a single SMA tube was modeled using finite element analysis (FEA). Transverse loading similar to the actual tube loading was applied by compressing the SMA tube in between two rigid plates as shown in Figure 4. The following boundary conditions were considered for the FEA: the plates were constrained to only move in the vertical direction along the vertical ( $x_2$ ) axis, the tube at the center along the horizontal ( $x_1$ ) axis was constrained to move only in the vertical direction. At the points of contact between the tube and the rigid plates the tube was constrained to only move in the vertical direction. An incremental point load of maximum 160N was applied to the top plate and the tube finite element mesh was created using 1000 2D-quadratic generalized plain strain elements. A user

material subroutine (UMAT) was used to model the SMA constitutive behavior in a commercial FEA package ABAQUS (HKS, 1997). The SMA constitutive model used for the FEA is a fully coupled thermo-mechanical model and has been presented in (Lagoudas et al., 1996; Lagoudas and Bo, 1999). The reader is referred to Qidwai and Lagoudas (2000) for explanation of the numerical algorithms developed for modeling the SMA constitutive response using UMAT. The FEA was performed on an IBM Regatta p690 supercomputer running Digital Unix V4.0E.

Figure 5 shows the tube in an intermediate deformation state after 80N load has been applied. Figure 6 shows the deformed tube under full 160N loading. Figure 6 also shows the amount of phase transformation

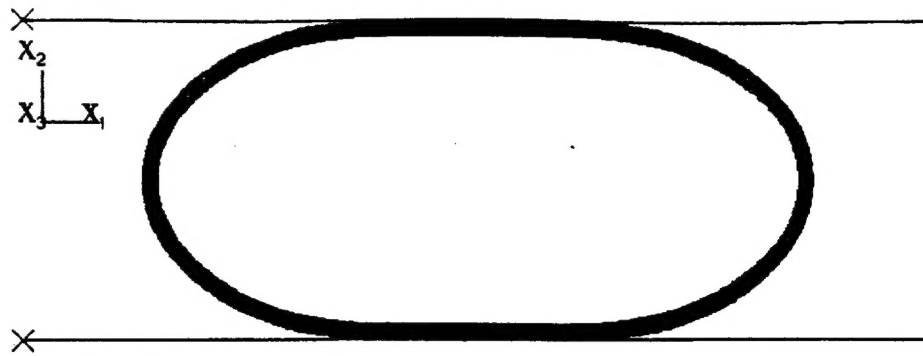


Figure 5. Partially deformed configuration of a SMA tube under transverse loading.

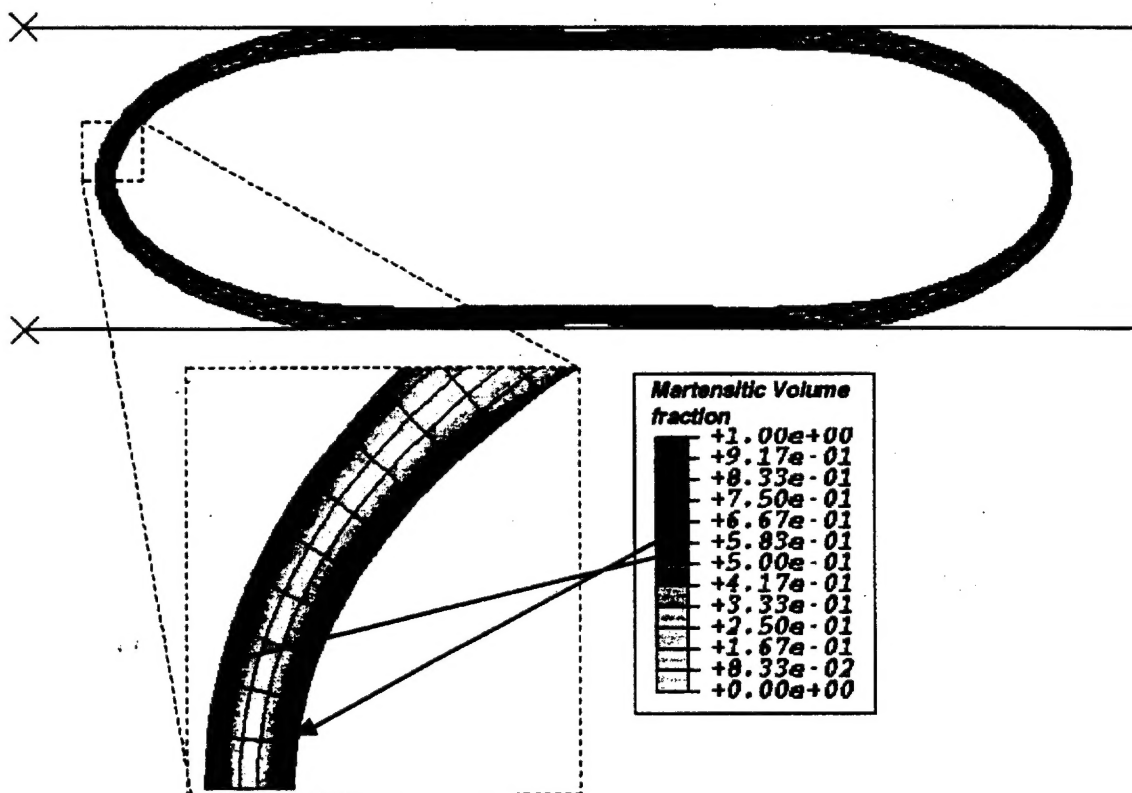


Figure 6. Deformed SMA tube configuration with martensitic volume fraction shown for high-stress concentration areas.

or the martensitic volume fraction of the deformed tube and illustrates limited phase transformation in small areas around the contact points between the tube and the loading plates and at outer and inner surfaces at points of stress concentrations (magnified in Figure 6). Results of the FEA shows less than 3% of the tube cross section undergoing phase transformations with more than 50% of the material transforming into martensite mainly around the area shown in the magnification in Figure 6. An additional 5% of the tube cross section shows transformation of more than 10% near the tube and plate contact points.

Based on the experiments and the small amount of SMA transforming as a result of the FEA, the authors have concluded that even though locally the increase or

decrease in the SMA tube temperature due to latent heat of phase transformation may be significant especially under dynamic loading conditions, the overall structural response is not drastically affected. This is justified because heat conduction and heat convection to and from the tube will cause the tube to reach a steady-state temperature close to the ambient environment at steady-state dynamic response. And, as it will be shown later in Part II for a given input excitation loading, as frequency increases the amount of SMA tube undergoing phase transformation decreases. Hence, temperature effects are assumed to be negligible for the SMA tubes used in this work.

Details of the vibration isolation test setup along with experimental results will be presented in Part II of this

two-part paper. Figures 2–6 have been introduced to show the difficulty in efficiently modeling such a SMA structural response for performing design optimization of the vibration isolation device along with experimental correlations and simulation of the dynamic system using the constitutive models mentioned in the previous section. Hence a Preisach hysteresis model (system ID-based model) was identified for the SMA tube response and will be presented in the following section.

## MODEL DESCRIPTIONS

### Preisach Model Adaptation for Pseudoelastic SMA Tube (Spring) Response

The classical Preisach model as stated earlier can be expressed as a weighted combination of relay operators. Figure 7(a) shows a classical Preisach hysteresis relay operator  $H_{\alpha\beta}[\delta(t)]$ . The relay operator can be explained by a rectangular loop where  $\alpha$  and  $\beta$  correspond to “up” and “down” switching values of the input respectively and it is assumed that  $\alpha \geq \beta$ . The rectangular loop can also be associated as a simplified representation of actual pseudoelastic SMA response. Works done by Webb (Webb, 1998; Webb et al., 1998) have shown that a Krasnoselskii–Pokrovskii (KP) (Krasnoselskii and Pokrovskii, 1983) type of hysteresis operator, gives a better representation of SMA response. The KP type operator is a smooth hysteretic operator with continuous branches rather than jump discontinuities like the Preisach operator. However, in this work, the developed model would be used to solve a SDOF system to simulate a dynamic system response. As a first step, a modified Preisach operator was implemented to account for pseudoelastic SMA spring element response rather than the KP operator.

The classical Preisach operator output is either +1 or -1 based on the value of the input. The operator output and input values are governed by the position of the

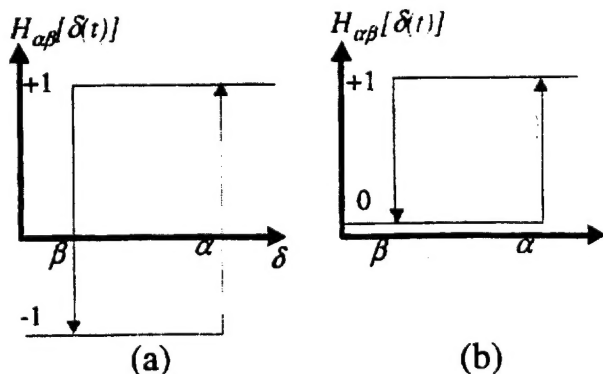


Figure 7. (a) Classical hysteresis operator; (b) modified hysteresis operator.

system or material response in the planar quadrants. As shown in Figure 3, the SMA pseudoelastic response can be represented either in the first or the third quadrant depending on the SMA element response undergoing tension or compression. In this work, the SMA element response corresponds to SMA tube undergoing compression under transverse loading. Therefore, the output value of the hysteresis operator used in this work has been modified to 0 or 1, as shown in Figure 7(b).

The mathematical form of the classical Preisach model is given as

$$f^{\text{SMA}}(t) = \iint_{\alpha \geq \beta} \mu(\alpha, \beta) H_{\alpha\beta}[\delta(t)] d\alpha d\beta \quad (1)$$

where  $\delta(t)$  is the input and represents displacement for the SMA spring elements,  $H_{\alpha\beta}[\delta(t)]$  represents hysteresis relay operators with different  $\alpha$  and  $\beta$  values containing the hysteresis effects and depends on  $\delta(t)$ . Here  $\alpha$  and  $\beta$  correspond to increasing and decreasing values of displacement.  $\mu(\alpha, \beta)$  represents the weighting function in the Preisach model, it describes the relative contribution of each relay to the overall hysteresis and  $f^{\text{SMA}}(t)$  is the output representing force generated by the SMA spring element and depends on the displacement history. The double integration presented in Equation (1) can be interpreted as a parallel summation of weighted relays as shown in Figure 8.

The weighting function  $\mu(\alpha, \beta)$ , also referred in the literature as the Preisach function is described over a region  $P$ , this region is referred to as the Preisach plane, where each point in  $P$  represents a unique relay. Based on the explanation given on the Preisach Model in Mayergoyz (1991); Hughes and Wen (1994) and Gorbet et al. (1998), the weighting function is defined over displacement (input) range, i.e., the domain of hysteresis exists between  $\delta_{\min}$  and  $\delta_{\max}$ .  $\alpha$  and  $\beta$  represents increasing and decreasing displacement values respectively, where the upper bound on  $\alpha$  is given by  $\delta_{\max}$  and the lower bound on  $\beta$  is given by  $\delta_{\min}$ . These two conditions along with the condition given in Equation (1), which defines the double integration to exist over a surface where  $\alpha \geq \beta$ , restricts  $P$  to a triangle. Figure 9

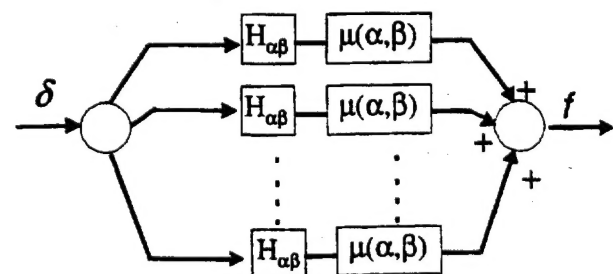


Figure 8. Schematic of Preisach model.

shows the schematic of the Preisach plane adapted for the work presented in this paper.

It must be noted that, according to Figure 7(b),  $H_{\alpha,\beta}[\delta(t)]$  can only take the values 0 and 1 (only in tension or compression of the SMA spring element). Thus, Equation (1) reduces to

$$f^{\text{SMA}}(t) = \iint_{S^+(t)} \mu(\alpha, \beta) d\alpha d\beta \quad (2)$$

where  $S^+$  is the region (shaded region shown in Figure 10 where  $\alpha \geq \beta$ ) containing all the relay operators in +1 state at time  $t$ . The other relays outside the shaded area

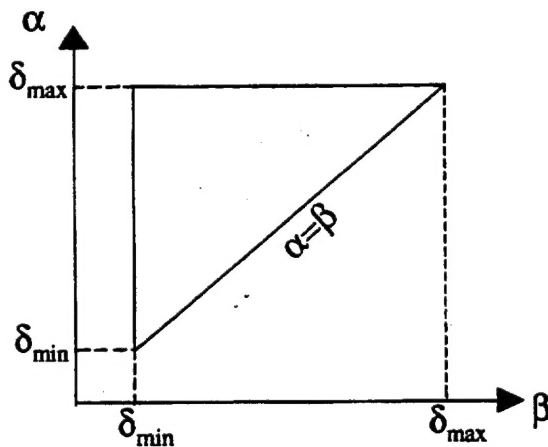


Figure 9. The Preisach plane.

are in zero state. There is a one-to-one correspondence between the relays  $H_{\alpha,\beta}$  and the points  $(\alpha, \beta)$  within triangle area where  $(\alpha \geq \beta)$ .

Figure 10 shows the geometrical interpretation of the Preisach model, it can be seen that the integration support area is changing with input extrema. Not all the input extrema are remembered by the model. The input maximum wipes out the vertices whose  $\alpha$  coordinates are below this input, and each input minimum wipes out the vertices whose  $\beta$  coordinates are above this minimum. This is the *wiping-out property* of the model and in essence shows the dependency of output on previous dominant input extrema. The loading path dependency as demonstrated by the pseudoelastic SMA response is represented by the wiping-out property of the Preisach model.

As the input increases, a horizontal line moves in the positive  $\alpha$  direction in  $S$ , changing all the relay outputs below the line to +1 state. As the input decreases, a vertical line moves in the negative  $\beta$  direction in  $S$ , changing all the relay outputs to the right of the line all to 0 state.

As shown in Figure 10, at the starting point  $t_0$ , the input is at zero and all the relay outputs are in zero (Figure 10(a)) state. As the input increases to  $\alpha_1$  at  $t_1$ , a horizontal line moves to  $\alpha_1$  from zero, the outputs of the relays above the line switch to +1 (Figure 10(b)). From  $t_2$  to  $t_3$ , the input is lowered to  $\beta_1$ , a vertical line sweeps down to  $\beta_1$  changing some relay outputs back to zero (Figure 10(c)). When the input is increased again to  $\alpha_2$ , some relays are changed to +1 (Figure 10(d)).

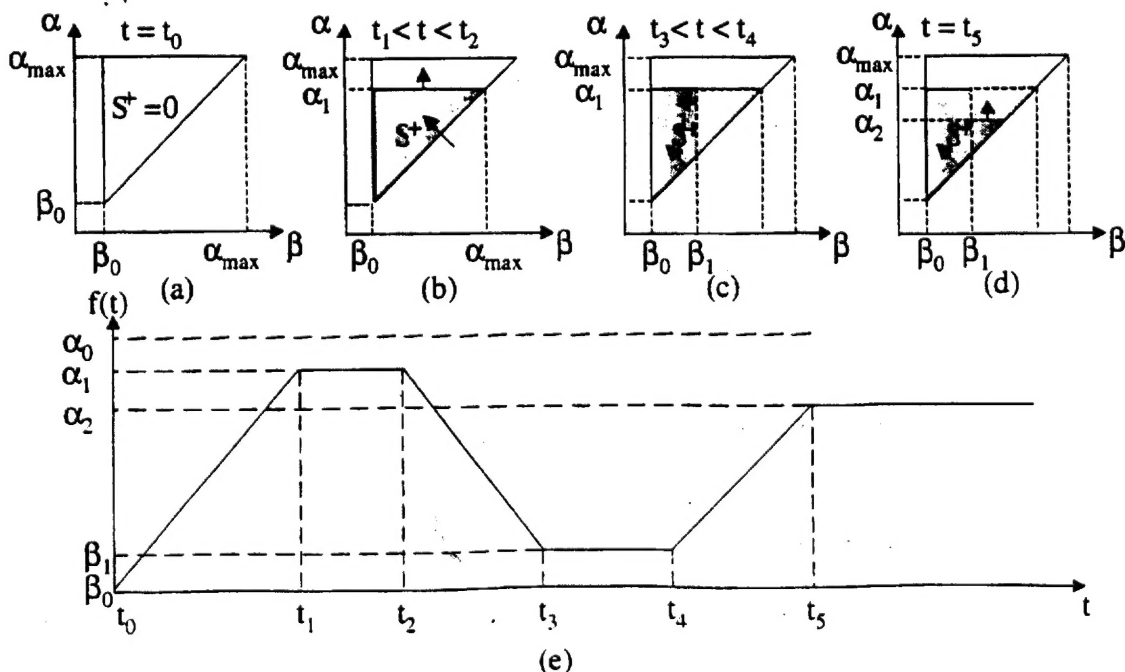


Figure 10. Evolution of outputs over the Preisach plane.

The output  $f^{\text{SMA}}(t)$  at each time  $t$  is simply the integral of  $\mu(\alpha, \beta)$  over  $S$  weighted by the corresponding relay outputs. A constant input will keep the output constant as well.

Another characteristic property of the classical Preisach model is called the *congruency property*. If the input continues to vary between two consecutive values, from Figure 10, it can be shown that the output would vary periodically as well. The two Preisach model properties mentioned above constitute the necessary and sufficient conditions for a nonlinear history-dependent hysteresis to be represented by the Preisach model. The reader is referred to Mayergoyz (1991) for further explanations on the classical Preisach model.

### IDENTIFICATION OF THE PREISACH FUNCTION

The Preisach function or the weighting surface for any hysteretic system, in this case a SMA spring element, can be easily determined from experimental data. This experimental data must contain what is defined as the "first-order transition (FOT) curves. The procedure is as follows. First, the input  $\delta(t)$  is brought to its minimum  $\delta_{\min}$  which is represented as  $\beta_0$  in Figure 11(a). Then monotonically increased to some value  $\alpha_1$ , as the input is increased from  $\delta_{\min}$ , an ascending branch of a major loop is followed, which is also referred to as a limiting branch in the literature (Mayergoyz, 1991).  $f_{\alpha_1}$  represents the output corresponding to  $\alpha_1$ , the input is now decreased monotonically to a value  $\beta_1$  and the corresponding output is described as  $f_{\alpha_1, \beta_1}$ . The term first-order describes that such curves are obtained after the first reversal of input, note that FOT can also be obtained by first-order descending curves as well. The corresponding  $\alpha$ - $\beta$  diagram is shown in Figure 11(b). To derive the weighting function in terms of FOT curves we introduce a function  $F(\alpha, \beta)$ ,

$$F(\alpha_1, \beta_1) = f_{\alpha_1} - f_{\alpha_1, \beta_1} \quad (3)$$

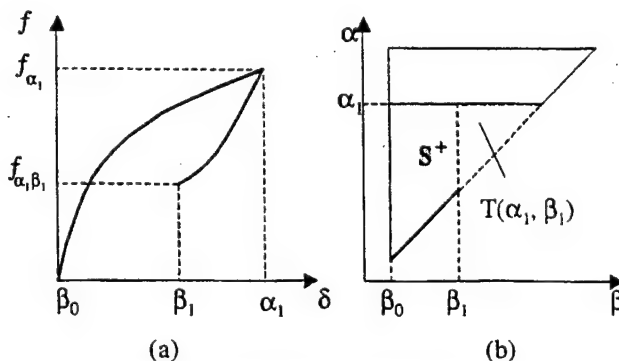


Figure 11. Schematic of identification input.

which represents the change in force as the displacement changes from  $\alpha_1$  to  $\beta_1$ . Equation (3) can also be represented as

$$F(\alpha_1, \beta_1) = \iint_{T(\alpha_1, \beta_1)} \mu(\alpha, \beta) d\alpha d\beta \quad (4)$$

The weighing function is obtained by taking the partial derivatives of Equation (4).

$$\mu(\alpha_1, \beta_1) = -\frac{F(\alpha_1, \beta_1)}{d\alpha_1 d\beta_1} \quad (5)$$

However, in order to avoid the double numerical differentiation of  $F(\alpha_1, \beta_1)$  to obtain  $\mu(\alpha_1, \beta_1)$ , the function  $F(\alpha_1, \beta_1)$  itself, is used to obtain the expression for the force, rather than Equation (2). This helps in avoiding amplifying errors in the experimental data and simplifies the numerical implementation of the Preisach model. Note that the  $F(\alpha, \beta)$  function can also be addressed as the FOT function.

### DERIVATION FOR NUMERICAL IMPLEMENTATION

Explicit expressions for force in terms of  $F(\alpha, \beta)$  can be subdivided into subcases based on increasing and decreasing displacement. For an increasing displacement (Figure 12(a)),  $f^{\text{SMA}}(t)$  is a double integral of the weighted function  $\mu(\alpha, \beta)$  on a region circumscribed by a set of links whose final segment is a horizontal line as shown in Figure 12(b). Starting from Equation (2) we can represent  $f^{\text{SMA}}(t)$  as

$$\begin{aligned} f^{\text{SMA}}(t) &= \iint_{S_1(t)} \mu(\alpha, \beta) d\alpha + \iint_{S_2(t)} \mu(\alpha, \beta) d\alpha \\ &\quad + \iint_{S_3(t)} \mu(\alpha, \beta) d\alpha d\beta \\ &= [F(\alpha_1, \beta_0) - F(\alpha_1, \beta_1)] + [F(\alpha_2, \beta_1) - F(\alpha_2, \beta_2)] + F(\delta(t), \beta_2) \\ &= \sum_{k=1}^N [F(\alpha_k, \beta_{k-1}) - F(\alpha_k, \beta_k)] + F(\delta(t), \beta_k) \quad (6) \end{aligned}$$

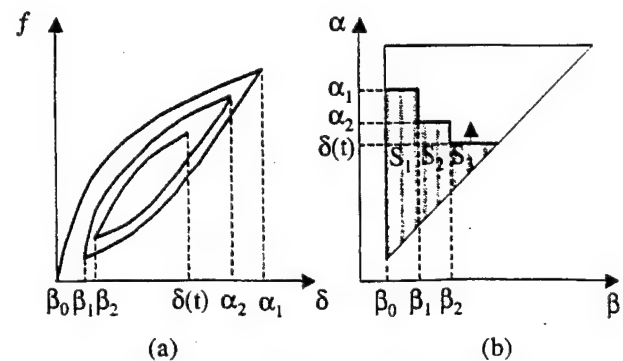


Figure 12. Schematic for increasing input.

where the integration is equivalent to summation of the trapezoids within the  $S^+(t)$  region, which can be generalized as shown in Equation (6).

Similarly, for decreasing displacement as shown in Figure 13(a),  $f^{SMA}(t)$  is a double integral of the weighted function  $\mu(\alpha, \beta)$  on a region circumscribed by a set of links whose final segment is a vertical line as shown in Figure 13(b). Starting from Equation (2) we can represent  $f^{SMA}(t)$  as

$$\begin{aligned} f^{SMA}(t) &= [F(\alpha_1, \beta_0) - F(\alpha_1, \beta_1)] + [F(\alpha_2, \beta_1) - F(\alpha_2, \beta_2)] \\ &\quad + [F(\alpha_3, \beta_2) - F(\alpha_3, \delta(t))] \\ &= \sum_{k=1}^{N-1} [F(\alpha_k, \beta_{k-1}) - F(\alpha_k, \beta_k)] \\ &\quad + [F(\alpha_N, \beta_{N-1}) - F(\alpha_N, \delta(t))] \end{aligned} \quad (7)$$

Equations (6) and (7) give the necessary increasing and decreasing displacement expression in terms of the measured FOT data.

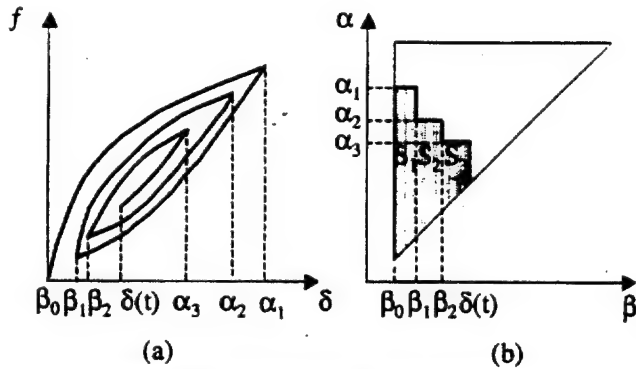


Figure 13. Schematic for decreasing input.

#### FIRST-ORDER TRANSITION (FOT) DATA COLLECTION AND MODEL IDENTIFICATION

In order to perform the first-order transition (FOT) data collection a pseudoelastic SMA tube (spring element) was loaded in the transverse direction in compression. The SMA tube was subjected to a range of displacements  $[0, 4]$  mm which corresponds to  $[\delta_{min}, \delta_{max}]$  and represent the lower and upper bound on displacements. The displacement range was subdivided into 13 subranges of orders pairs  $\{\delta_i\}_{i=0, \dots, n}$ , leading to  $n/2(n+1)$  FOT data points for all pairs  $(\delta_i, \delta_j)$  with  $j \leq i$ . Force-displacement tests were performed on an MTS servo-hydraulic load frame with a TestStar II m controller under displacement control at 25°C. The displacement input used for the FOT curves is given in Figure 14 and the corresponding force-displacement diagram is shown in Figure 15. Figure 16 shows a 3-D plot of the FOT data obtained from Figure 14.

Theoretically greater amount of FOT curves collected lead to more accurate hysteresis modeling, however this amounts to greater memory storage requirements and lower computational efficiency. Hence a trade-off needs to be exercised on accuracy compared to computational efficiency. The effects of choosing less number of FOT data points are shown in Figures 17 and 18, where Preisach models identified by using 15 and 45 data points are shown. This corresponds to subdividing the input displacement range into 5 and 9 subdivisions with a difference of 1.0 mm and 0.50 mm respectively. Since the objective is to have a computationally efficient model for predicting dynamic response without compromising on accuracy and computational efficiency 91 FOT data points have been considered for the final identification. This was the reason for having the

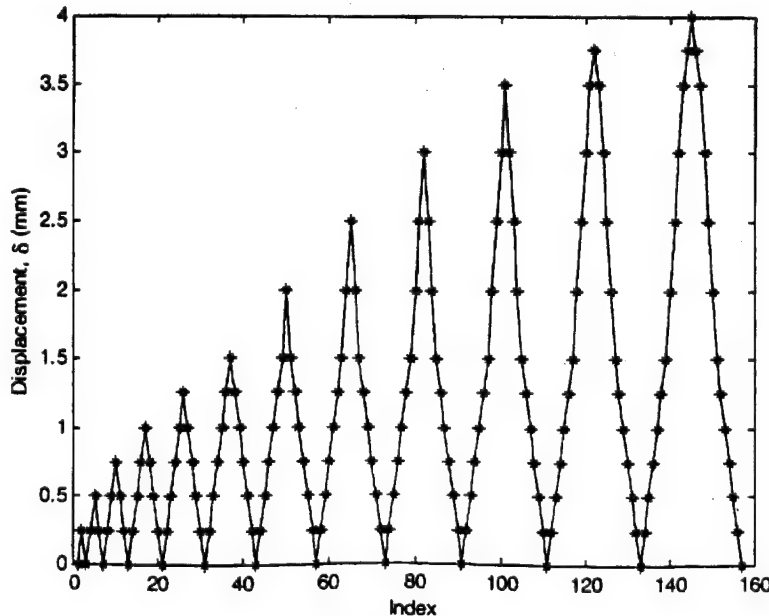


Figure 14. Identification displacement (input).

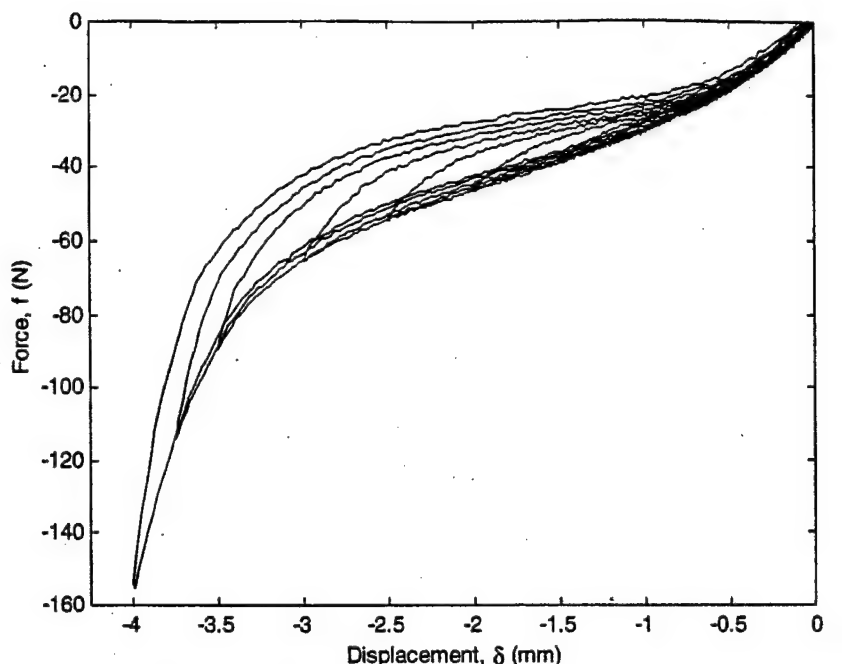


Figure 15. Experimental first-order transition (FOT) curves.

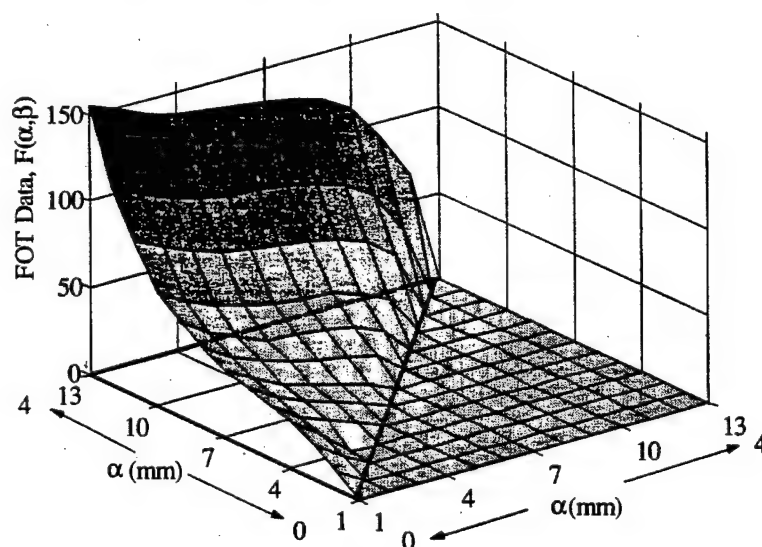


Figure 16. Experimental first-order transition (FOT) data.

displacement range subdivided into 13 subranges. Figure 19 shows the experimental data along with the 91 data points used to generate  $F(\alpha, \beta)$  function. The Preisach model simulated using the  $F(\alpha, \beta)$  function is also shown in Figure 19.

#### FIRST-ORDER TRANSITION (FOT) DATA NUMERICAL INTERPOLATION

To account for input displacements which do not correspond to any stored FOT curves, numerical interpolation is required to find out the output force. Figure 20 shows a schematic of the Preisach plane, where the  $\alpha, \beta$  mesh represents experimentally identified FOT data

points. A typical displacement input which does not correspond to any stored FOT data points is also shown on the Preisach plane. At first, the interpolation procedure relies on identifying the history of the input  $\alpha_k, \beta_k$ . This is followed by identifying the rectangular or triangular cell to which  $\alpha_k, \beta_k$  belong. A linear interpolation is used to evaluate  $F(\alpha_k, \beta_k)$ . Equation (8) represents the rectangular cell case, where the coefficients  $r_{i=1, \dots, 4}$  are obtained for each rectangular cell, by solving equations of the form given in Equation (8) for each vertex of the rectangular cell.

$$F(\alpha_k, \beta_k) = r_1 + r_2\alpha_k + r_3\beta_k + r_4\alpha_k\beta_k \quad (8)$$

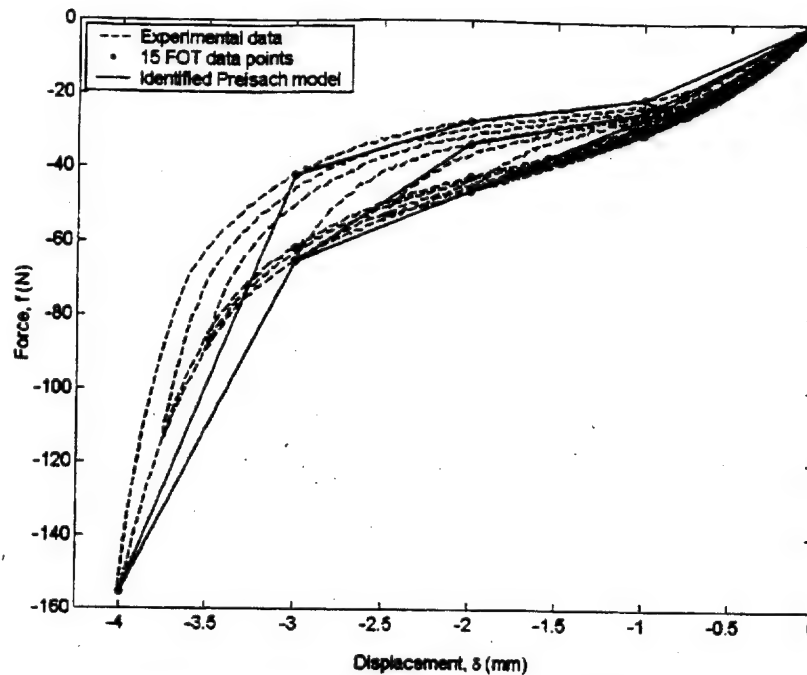


Figure 17. Identified Preisach model using 15 data points.

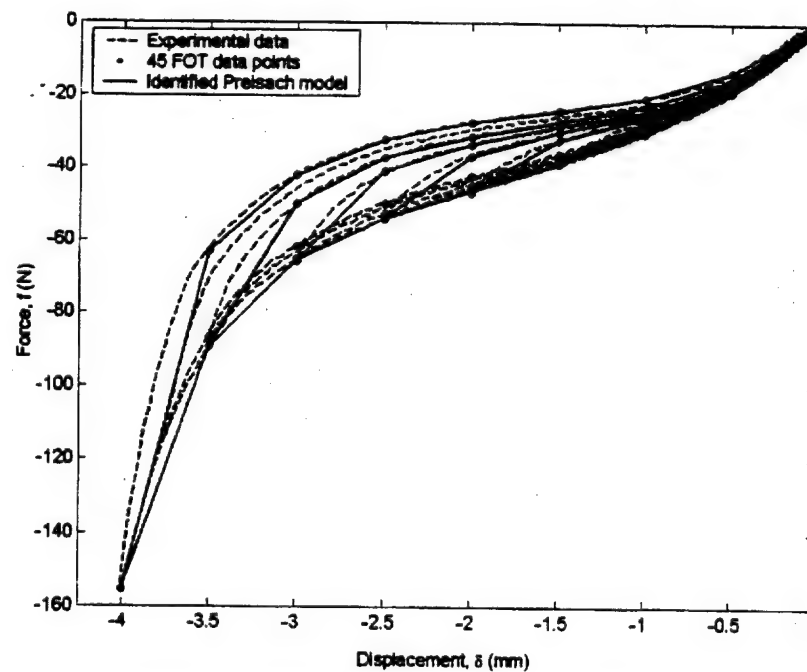


Figure 18. Identified Preisach model using 45 data points.

Equation (9) represents the triangular cell case, where the coefficients  $t_{i=1, \dots, 3}$  are obtained for each triangular cell, by solving equations of the form given in Equation (9) for vertices of the triangular cell.

$$F(\alpha_k, \beta_k) = t_1 + t_2 \alpha_k + t_3 \beta_k \quad (9)$$

Figure 21 shows a random displacement input which does not contain any identified FOT data points, the corresponding response using the calibrated Preisach

model using 91 data points (see Figure 19) is shown in Figure 22.

#### Physically Based Simplified SMA Model for Pseudoelastic SMA Tube Response

In addition to accurately modeling and experimentally validating the SMA-based vibration isolation device mentioned earlier, another goal of this study was to numerically explore the effects of pseudoelasticity

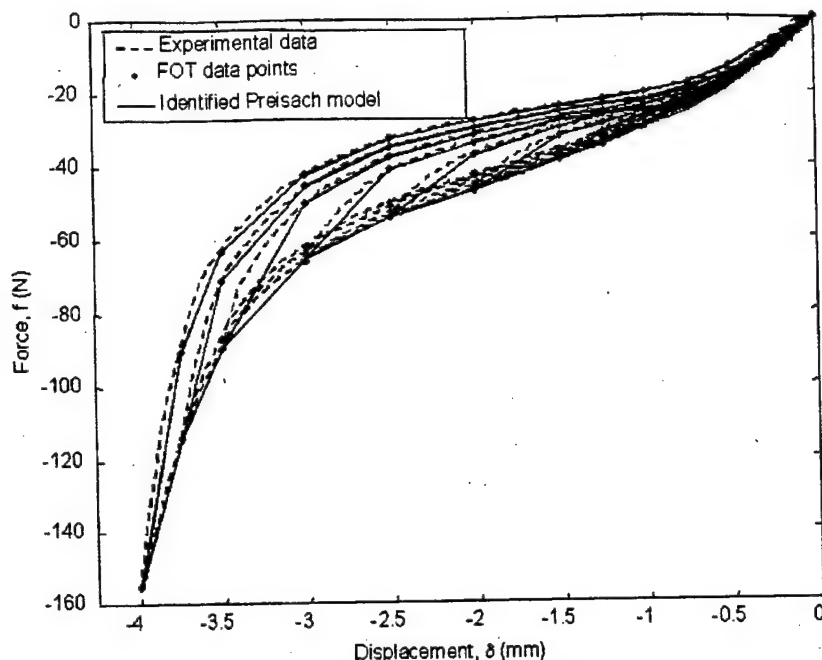


Figure 19. Identified Preisach model using 91 data points.

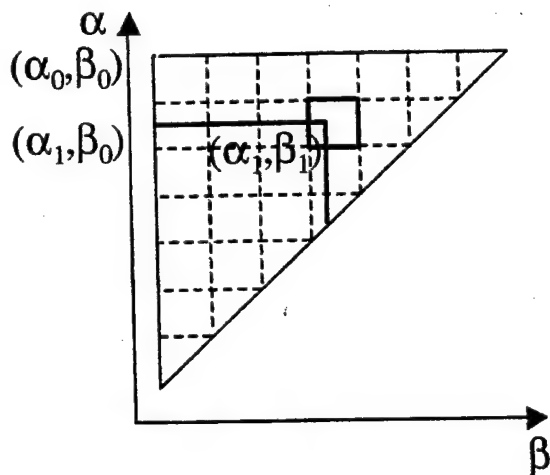


Figure 20. Numerical interpolation schematic.

on vibration isolation under a wide range of dynamic system conditions. To explore a broad range of system conditions like excitation amplitude, mass, number of SMA spring elements and initial conditions an efficient and qualitative representation of the SMA spring element force-displacement response with flexibility to change structural stiffness, hysteresis width, and operating temperature was needed. Therefore to aid in performing parametric studies a physically based simplified SMA model has also been calibrated based on the pseudoelastic SMA tube structural response and the following subsection discusses its development.

The simplified model is capable of predicting the behavior of a SMA spring element at temperatures above

the austenite finish temperature, ( $A^0_f$ ), the temperature at which the reverse transformation from martensite to austenite is complete. Additionally, this model is displacement driven and is dependent on the loading history to correctly predict the forward and reverse transformation behavior and the minor loop behavior of a SMA structure. The basis of the model is the assumption that the relationship between force and displacement in a SMA structure at temperatures above  $A^0_f$  can be represented by a series of linear segments. The model is based on earlier work done by Lagoudas et al. (2001b) and the following description extends the work presented in Lagoudas et al. (2001b) to account for force-displacement response of a SMA tube loaded in the transverse direction and modeled as a spring.

From a typical pseudoelastic force-displacement compression test (Figure 23) of the SMA tube used in the prototype device, performed at a temperature greater than  $A^0_f$ , the equivalent spring stiffness of the SMA structure in austenite ( $K_A$ ) and martensite ( $K_M$ ) can be obtained as well as the maximum value of transformation displacement ( $\delta_{max}^{tr}$ ). As mentioned earlier, the force-displacement test shown in Figure 23 is for a SMA tube used in the prototype device, which is loaded in compression in a transverse direction and should not be considered as SMA material response. Pseudoelastic SMA material response shows higher material stiffness in austenite compared to martensite. However, for the structural response shown in Figure 23, as the displacement increases, even though parts of the tube are undergoing phase transformation, due to the deformed geometry of the tube, the equivalent spring stiffness of the tube in the martensitic phase ( $K_M$ )

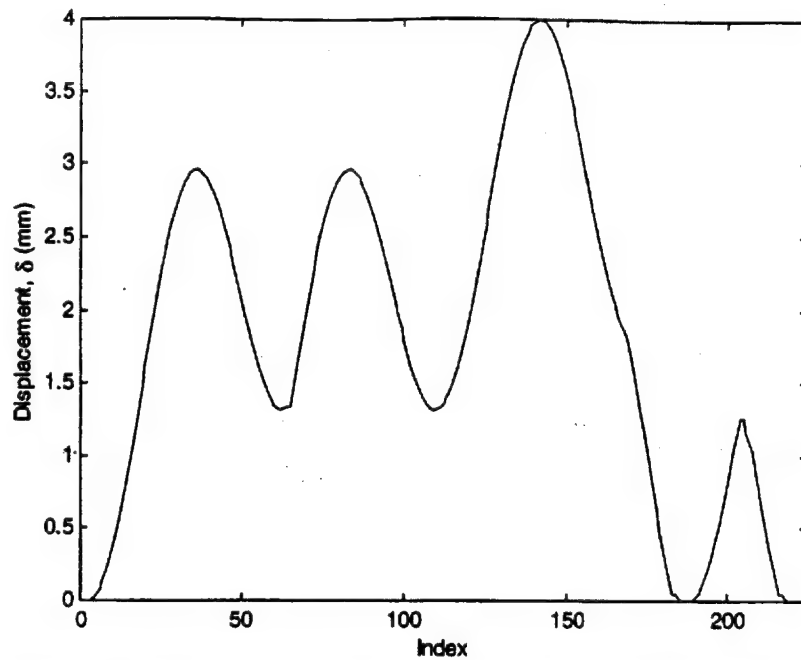


Figure 21. Random displacement input not corresponding to identified data points.

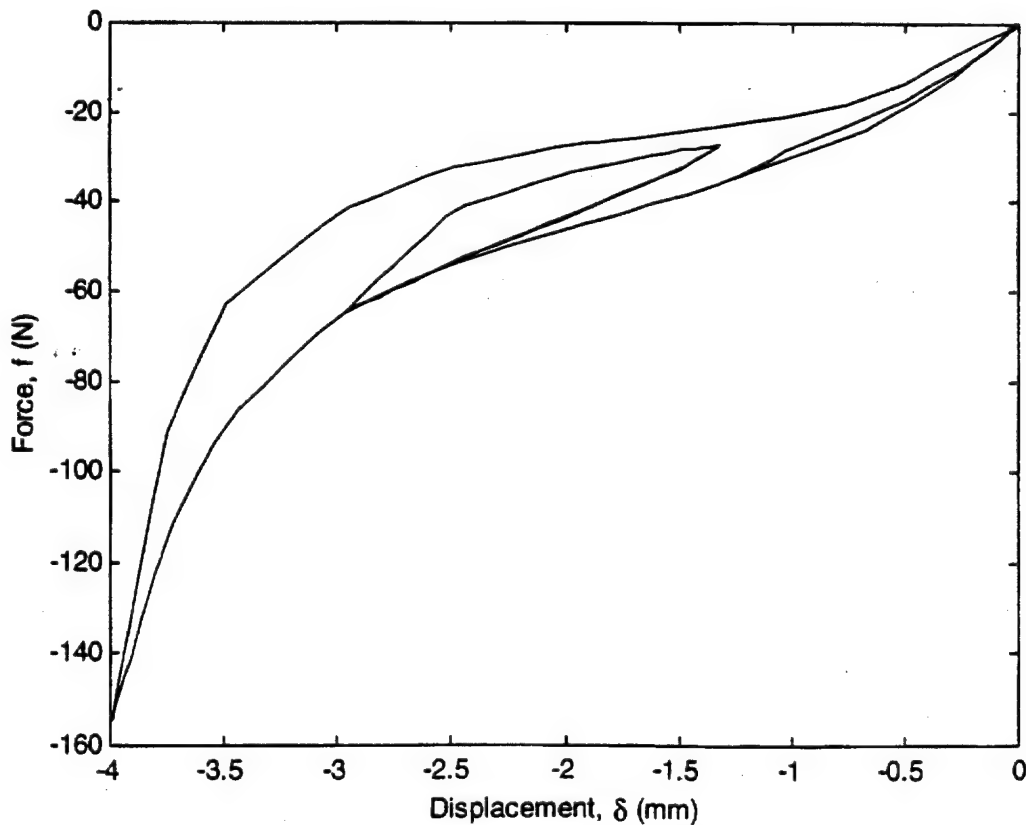
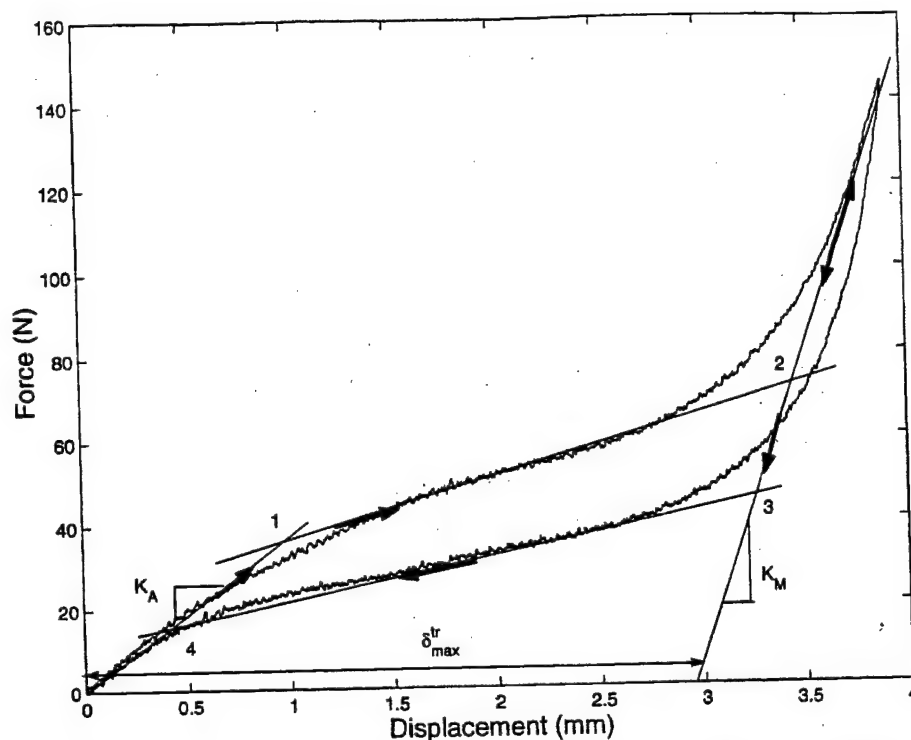


Figure 22. Calibrated Preisach model force-displacement response for random displacement input (Figure 21).

is greater than the equivalent spring stiffness of the tube in the austenitic phase ( $K_A$ ). Through the use of a Differential Scanning Calorimeter (DSC), the temperatures at which transformation occurs under zero stress can be determined.

For representation of force-displacement pseudoelasticity of a SMA structure, in this case SMA tubes, a structural force-temperature diagram describing the relationship between force, displacement, and the spring element phase can be constructed by one DSC



**Figure 23.** Pseudoelastic force-displacement response of a SMA tube with equivalent spring stiffness of austenite phase, equivalent spring stiffness of martensite phase, and transformation displacement labeled.

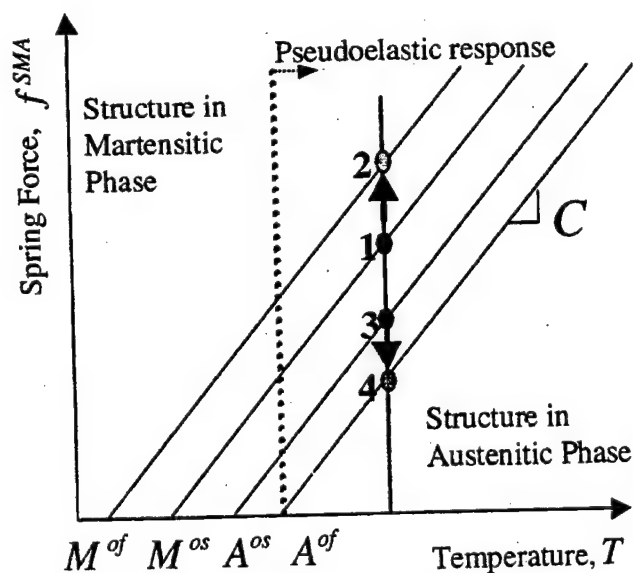


**Figure 24.** SMA spring element force-temperature diagram with pseudoelastic loading path.

measurement and one pseudoelastic response test, as shown in Figure 24. The assumption is made that the lines marking the transformation boundaries are parallel, which strictly speaking is not necessarily correct but for the purpose of this model it does allow for a simplified representation of the pseudoelastic response. In this case, the zero stress transformation temperatures and the slope of the transformation boundaries are chosen based on the pseudoelastic response and the DSC tests, but modified slightly so that

the pseudoelastic force-displacement relationship is preserved for the structure. Another simplification is in the selection of the transition points between elastic loading and transformation. Due to the nonuniform stress state and polycrystalline nature of SMA tubes, some areas of the material begin to transform before others, resulting in the smooth transitions seen in Figure 23. However, the simplified model presented here requires specific transition points (Points 1-4 in Figures 23-25) at which to begin and end the forward

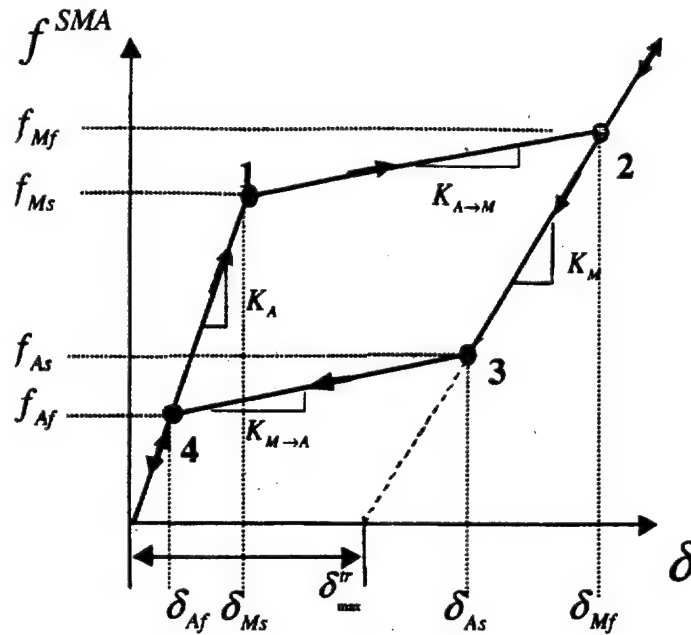


Figure 25. Calculated pseudoelastic force-displacement response of SMA.

and reverse transformation, hence, points are chosen so that the pseudoelastic force-displacement relationship is preserved. Once the simplifications are made and the appropriate constants are chosen, the simplified model utilizes the force-temperature diagram (Figure 24) to create a piecewise linear representation of the pseudoelastic response of the SMA spring (tube) element shown in Figure 23.

From the force-temperature diagram, and given that the temperature of the SMA is known and constant, it is possible to calculate the forces at which the forward and reverse transformations begin and end from Equation (10) where  $f'$  is the force,  $C$  is the slope of the transformation boundary in the force-temperature plane,  $T$  is the temperature, and  $T_i$  is the zero-stress transition temperature determined from the DSC results for the respective transition.

$$f' = C(T - T_i) \quad (10)$$

Additionally, the constitutive relation for SMA can be modified to yield Equation (11), where  $K_p$  is the respective stiffness of either austenite, martensite, or a mixture of the two phases,  $\delta$  is the total applied displacement and  $\delta^{tr}$  is the transformation displacement of the SMA. Transformation displacement for a force-displacement model is equivalent to the transformation strain for a stress-strain model.

$$f = K_p(\delta - \delta^{tr}) \quad (11)$$

Given that the material state is assumed to be known at the beginning and end of transformation for both

forward and reverse transformations, one can calculate the displacement at which transformation will occur. Using this data, one can construct the following force-displacement diagram as shown in Figure 25 using only the material parameters mentioned above. For this simplified model of pseudoelastic loading, the transitions delineating the beginning and end of forward and reverse transformation are dependent only upon the ambient temperature and the material parameters, including the zero load transition temperatures, the transformation displacement and the stiffness of the two phases. For the beginning of the austenite to martensite, or forward, transformation (Point 1 on Figure 25), the corresponding force and displacement are calculated from Equations (12) and (13).

$$f_{Ms} = C(T - M^{0s}) \quad (12)$$

$$\delta_{Ms} = \frac{C(T - M^{0s})}{K_A} \quad (13)$$

For the end of the forward transformation (Point 2), the corresponding force and displacement are calculated from Equations (14) and (15).

$$f_{Mf} = C(T - M^{0f}) \quad (14)$$

$$\delta_{Mf} = \frac{C(T - M^{0f})}{K_M} \quad (15)$$

For the beginning of the martensite to austenite, or reverse, transformation (Point 3), the corresponding

force and displacement are calculated from Equations (16) and (17).

$$f_{As} = C(T - A^{0s}) \quad (16)$$

$$\delta_{As} = \frac{C(T - A^{0s})}{K_M} \quad (17)$$

For the end of the reverse transformation (Point 4), the corresponding force and displacement are calculated from Equations (18) and (19).

$$f_{Af} = C(T - A^{0f}) \quad (18)$$

$$\delta_{Af} = \frac{C(T - A^{0f})}{K_A} \quad (19)$$

Assuming piecewise linear response and combining all of this information together will result in completely determining the force-displacement response of a SMA for a full loading induced transformation cycle, as shown schematically in Figure 25. The effects of latent heat due to the rate-dependent release and absorption of heat during pseudoelastic phase transformations can be explicitly accounted for by choosing different slopes and transformation points for the piecewise linear simplified SMA model.

### MAJOR LOOP RESPONSE

To correctly predict the force-displacement response of a SMA, the loading path for full transformation, or the major loop, must be modeled. For the simplified SMA model, this is accomplished by assuming that both the transformation displacement,  $\delta^{tr}$ , and the force,  $f$ , vary linearly during transformation and that the force corresponds to displacement in a linear manner when transformation is not occurring. As a result, the SMA material can be modeled as a series of straight lines in force-displacement space, where the intersection of these lines correspond to the transition between elastic loading and transformation for forward and reverse transformation. This can be illustrated schematically, as shown in Figure 25. For elastic loading in the austenite region ( $4 \rightarrow 1$ ), prior to the beginning of forward transformation, the transformation displacement remains zero and the force is directly related to the displacement. This is explicitly stated in Equations (20) and (21).

$$\delta^{tr} = 0 \quad (20)$$

$$f^{SMA} = K_A \delta \quad (21)$$

For forward transformation, the region between Points 1 and 2, the transformation displacement varies linearly

between zero and the maximum value of transformation displacement,  $\delta_{max}^{tr}$ . Additionally, the force level also varies linearly between the force levels corresponding to the beginning and end of transformation. Mathematically this is shown below in Equations (22) and (23).

$$\delta^{tr} = \delta_{max}^{tr} \left( \frac{\delta - \delta_{Ms}}{\delta_{Mf} - \delta_{Ms}} \right) \quad (22)$$

$$f^{SMA} = f_{Ms} + \frac{\delta^{tr}}{\delta_{max}^{tr}} (f_{Mf} - f_{Ms}) \quad (23)$$

At displacement levels above the martensite finish level, the region after Point 2, the force again relates linearly to the displacement and the transformation displacement remains at a constant value equal to  $\delta_{max}^{tr}$ . This relation remains true even after the onset of unloading until the beginning of reverse transformation begins (Point 3) as shown in Equations (24) and (25).

$$\delta^{tr} = \delta_{max}^{tr} \quad (24)$$

$$f^{SMA} = f_{Mf} + K_M(\delta - \delta_{Mf}) \quad (25)$$

After the beginning of reverse transformation (Point 3), and before the transformation to austenite completes (Point 4), the transformation displacement again varies linearly, this time between  $\delta_{max}^{tr}$  and zero. Likewise the force varies linearly between the value at the start of reverse transformation and the value at the end of transformation. This is shown in Equations (26) and (27).

$$\delta^{tr} = \delta_{max}^{tr} - \delta_{max}^{tr} \left( \frac{\delta_{As} - \delta}{\delta_{As} - \delta_{Af}} \right) \quad (26)$$

$$f^{SMA} = f_{Af} + \frac{\delta^{tr}}{\delta_{max}^{tr}} (f_{As} - f_{Af}) \quad (27)$$

At the conclusion of reverse transformation, the transformation strain is again zero and the force again varies linearly with the displacement, as shown in Equations (20) and (21).

The force-displacement history for a major loop loading path for the simplified model is the same as shown in Figure 23.

The major loop SMA pseudoelastic schematic shown in Figure 25 can also be represented by using linear springs and slip or frictional elements and is referred to as mechanism-based nonlinear hysteretic response. Correlations between the simplified SMA model and mechanism-based nonlinear hysteretic response are presented in Appendix A for completeness.

### MINOR LOOP RESPONSE

To accurately model SMAs for a particular application, it becomes necessary to model the minor loop loading cycles. Minor loop loading cycles are those loading cycles that do not result in complete transformation from austenite to martensite and back to austenite. From inspection of Figure 26, which illustrates a minor loop displacement loading path, it becomes clear that in order to model this behavior, some modifications must be made to the equations above to account for this incomplete transformation. As a result of the simplicity of this model, the modifications are easy to implement. The first issue that must be dealt with is the dependence of the current SMA structural behavior on the history of loading

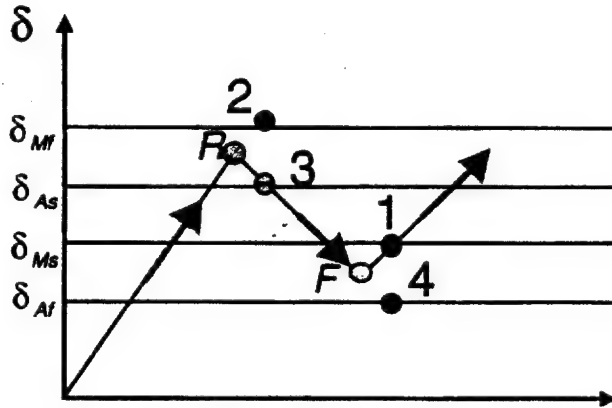


Figure 26. Displacement path for minor loop loading.

of the SMA component. This can be accomplished by storing the maximum and minimum values of force, displacement, and transformation displacement for the previous loading cycle. The second issue to be dealt with is the modification of the points in force-displacement space that initiate the beginning of forward and reverse transformation. The third issue relates to the stiffness of the SMA structure. As the SMA structure transforms between austenite and martensite, the stiffness of the structure changes between the structural stiffness of each phase. The stiffness at any given point during transformation is calculated using a rule of mixtures on the compliance (Reuss bound).

Figure 27 depicts a minor loop case. When loading from zero force in the austenite phase, the equations are the same as for the initial elastic loading and the forward transformation. However, for a minor loop loading path, the loading is reversed prior to completion of forward transformation at point *R*. At this point the maximum values of force, displacement, and transformation displacement are recorded, as they will be used in subsequent calculations. As unloading begins from point *R* to 3, initially there is no transformation, so that the unloading occurs elastically but at a stiffness that is neither the austenite stiffness nor martensite stiffness. Unloading occurs elastically from the maximum transformation point and the slope is determined by maximum degree of transformation obtained. For this portion of the force-displacement relation, the unloading stiffness,  $K_R$ , and the force are calculated as shown in Equations (28) and (29) where  $\delta_R^u$ ,  $f_R$ , and  $\delta_R$  are the values of transformation displacement, force, and

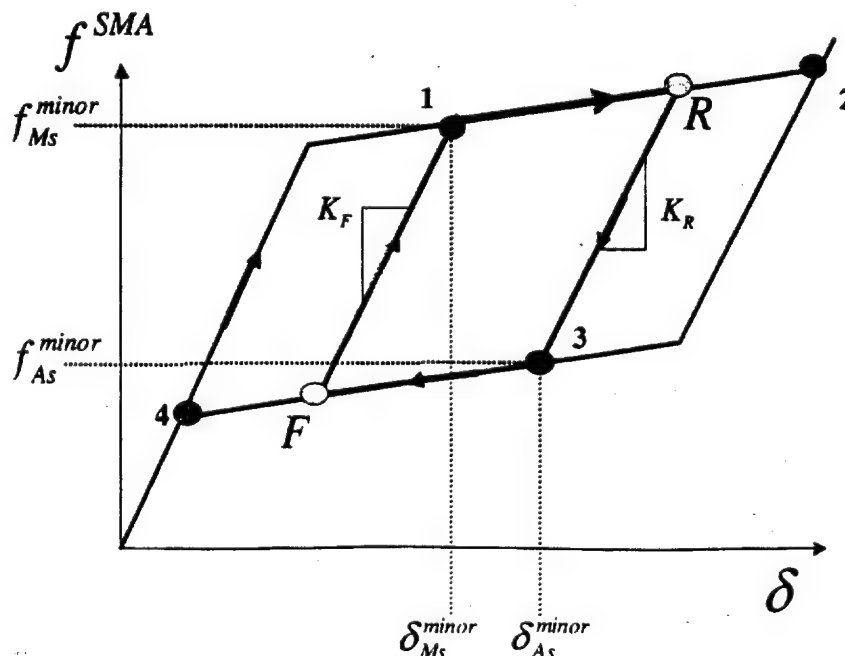


Figure 27. Force-displacement path for minor loop loading.

displacement recorded when the loading path changed directions.

$$K_R = \frac{K_M K_A}{\delta_R^{\text{tr}} / \delta_{\text{max}}^{\text{tr}} (K_A - K_M) + K_M} \quad (28)$$

$$f^{\text{SMA}} = f_R + K_R(\delta - \delta_R) \quad (29)$$

The transformation strain remains constant for this section of the loading path, since the unloading is elastic and no transformation occurs. As the SMA structure continues to unload, the path it is following will eventually intersect the line for major loop reverse transformation (Point 3), where reverse transformation begins for minor loop loading paths. Due to the incomplete forward transformation, this point is different from the  $(f_{As}, \delta_{As})$  pair denoting Point 3 in Figure 25 and is defined by Equations (30) and (31).

$$\delta_{As}^{\text{minor}} = \delta_{As} + \frac{\delta_R^{\text{tr}}}{\delta_{\text{max}}^{\text{tr}}} (\delta_{As} - \delta_{Af}) \quad (30)$$

$$f_{As}^{\text{minor}} = f_{As} + \frac{\delta_R^{\text{tr}}}{\delta_{\text{max}}^{\text{tr}}} (f_{As} - f_{Af}) \quad (31)$$

As this point is reached, reverse transformation begins and the following equations will determine the values of transformation displacement and force from Point 3 onwards.

$$\delta^{\text{tr}} = \delta_{\text{max}}^{\text{tr}} - \delta_{\text{max}}^{\text{tr}} \frac{\delta_{As}^{\text{minor}} - \delta}{\delta_{As}^{\text{minor}} - \delta_{Af}} \quad (32)$$

$$f^{\text{SMA}} = f_{Af} + \frac{\delta^{\text{tr}}}{\delta_{\text{max}}^{\text{tr}}} (f_{As}^{\text{minor}} - f_{Af}) \quad (33)$$

As the structure continues to unload, the force will decrease and the transformation displacement will go to zero as the material approaches Point 4 where reverse transformation ceases. At this point the SMA structure will be in austenite again and will unload elastically to zero load. Now, if the structure does not unload entirely into austenite, but again changes the loading direction and begins to load again, the force, displacement, and transformation displacement at this point must again be recorded. This point is shown as point *F* in Figures 26 and 27. As the material begins to load from point *F* to 1, it again loads elastically at a stiffness determined by the minimum degree to which transformation had progressed. The stiffness and force level are given in Equations (34) and (35) where  $\delta_F^{\text{tr}}$ ,  $f_F$ , and  $\delta_F$  are the values of transformation displacement, force, and displacement recorded when the loading path changed directions.

$$K_F = \frac{K_M K_A}{\delta_F^{\text{tr}} / \delta_{\text{max}}^{\text{tr}} (K_A - K_M) + K_M} \quad (34)$$

$$f^{\text{SMA}} = f_F + K_F(\delta - \delta_F) \quad (35)$$

From this point the SMA structure loads elastically until this loading path intersects with the forward transformation path for major loop loading (Point 1). This point is calculated in a similar manner to that used in the calculation of the beginning of reverse transformation and is again based on the intersection of the major loop loading path and the minor loop loading path. The formulas defining this point are given in Equations (36) and (37).

$$\delta_{Ms}^{\text{minor}} = \delta_{Ms} + \frac{\delta_F^{\text{tr}}}{\delta_{\text{max}}^{\text{tr}}} (\delta_{Mf} - \delta_{Ms}) \quad (36)$$

$$f_{Ms}^{\text{minor}} = f_{Ms} + \frac{\delta_F^{\text{tr}}}{\delta_{\text{max}}^{\text{tr}}} (f_{Mf} - f_{Ms}) \quad (37)$$

From this point, force and transformation displacement for forward transformation are calculated in a manner similar to that used in the calculation of force and transformation displacement for the reverse transformation. The equations are as follows:

$$\delta^{\text{tr}} = \delta_{\text{max}}^{\text{tr}} \frac{\delta - \delta_{Ms}^{\text{minor}}}{\delta_{Mf} - \delta_{Ms}^{\text{minor}}} \quad (38)$$

$$f^{\text{SMA}} = f_{Ms}^{\text{minor}} + \frac{\delta^{\text{tr}}}{\delta_{\text{max}}^{\text{tr}}} (f_{Mf} - f_{Ms}^{\text{minor}}) \quad (39)$$

The continuation of loading along this path will result in complete transformation to martensite as described in the major loop section. A change in loading direction prior to complete transformation will result in additional minor loops and the preceding equations are applicable. Figure 28 shows a typical displacement path that would result in minor loop loading. The resulting force-displacement response is shown in Figure 29.

#### CALIBRATION OF THE PHYSICALLY BASED SIMPLIFIED SMA MODEL BASED ON THE PSEUDOELASTIC SMA TUBE RESPONSE

In order to calibrate the simplified pseudoelastic SMA model presented here, the DSC data was combined with the results of a pseudoelastic compression test shown in Figure 24. As mentioned earlier, the mechanical test was performed on an MTS servo-hydraulic load frame with a TestStar II controller under displacement control and the DSC analysis was performed using a Perkin Elmer Pyris 1 Differential Scanning Calorimeter. The 10 mm long, 6 mm Nitinol SMA tube with a wall thickness of approximately 0.17 mm was loaded transverse to the longitudinal axis in increments up to approximately 70% reduction in diameter. Tests were performed at different temperatures ranging from 25 to 65°C,

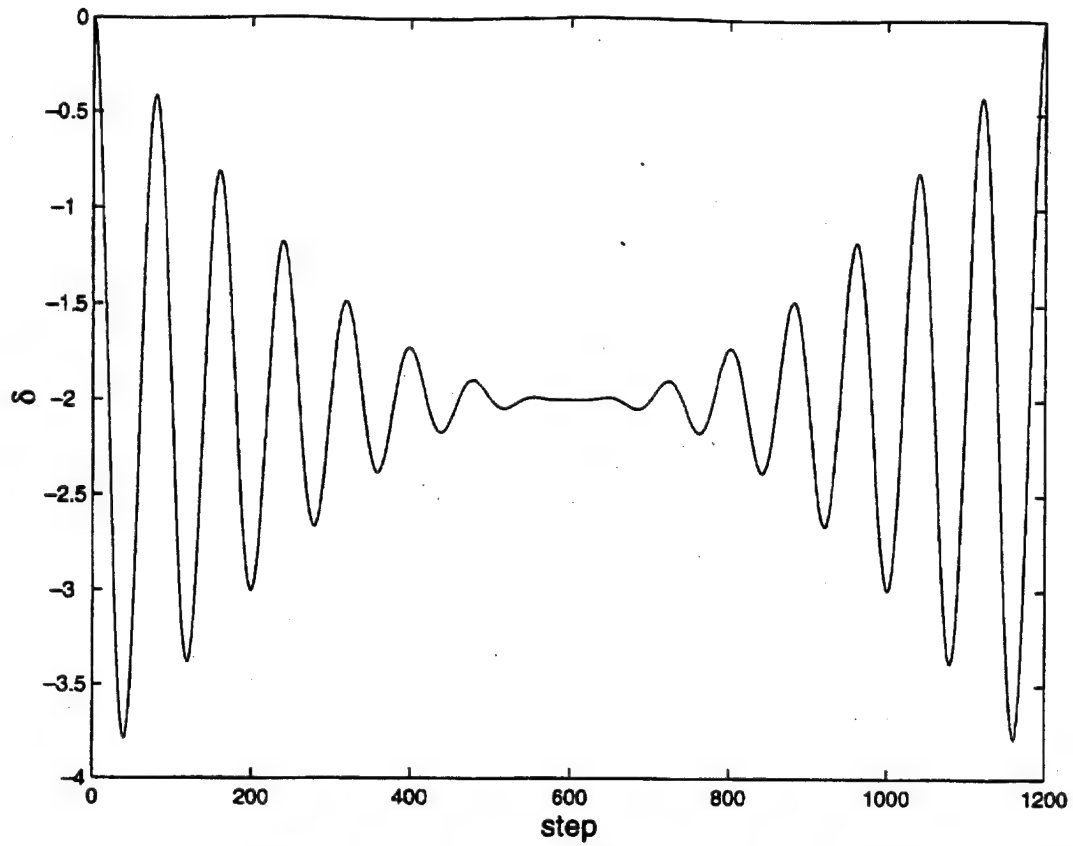


Figure 28. Minor loop loading input displacement path.

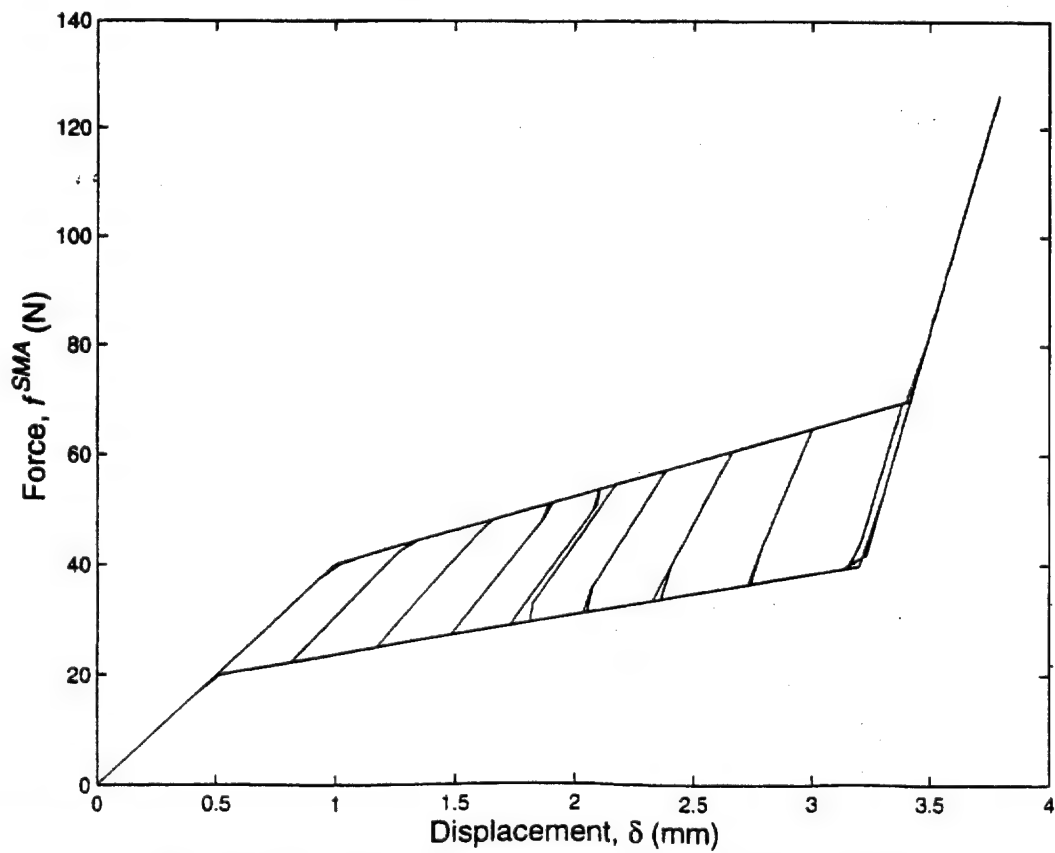


Figure 29. Response of simplified model for both major and minor loop loading.

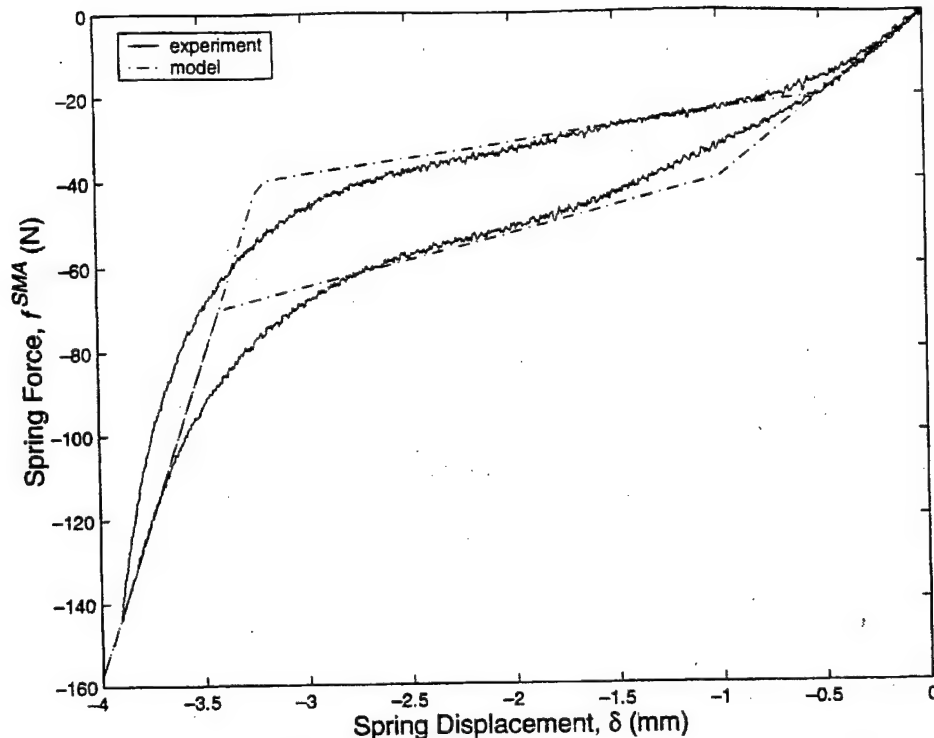


Figure 30. Force vs. displacement response of SMA compression spring element (tube) compared with the calibrated simplified SMA model.

all of which yielded similar results. The tube response showed maximum 5% of increased hardening at higher testing temperatures as higher stresses are required to induce phase transformations (Figure 1). The small change in the force-displacement curves for different temperatures was attributed to the fact that only some parts of the SMA tube were undergoing phase transformation as discussed in "Brief Description of the Experimental Setup and Finite Element Analysis" (see Figure 6).

Experimentally determined force-deflection behavior for the SMA spring, along with the output for the physically based SMA model as calibrated for use in this work, is shown in Figure 30. In order to calibrate the model for the SMA spring, it was necessary to implement the assumptions listed earlier concerning the beginning and end of transformation for both force displacement space and force temperature space. From the experimental data it is evident that the slope of the transformation regions in force temperature space are not parallel, however for this work a median value of  $5.7 \text{ N/}^\circ\text{C}$  was chosen. Additionally, it is obvious that for the SMA tube, that there is not a single point marking the beginning or ending of any of the transformation regions so it was again necessary to choose a point that would allow for the best representation of the force-displacement response. As a result of these assumptions it was then necessary to modify the zero load transformation temperatures slightly from the values measured during the DSC tests. The values used to calibrate the model are shown in Table 1 and as shown

Table 1. Experimentally determined parameters for SMA model.

$M^{\text{tr}} = 12.7^\circ\text{C}$	$K_A = 40 \text{ kN/m}$
$M^{\text{cs}} = 17.9^\circ\text{C}$	$K_M = 150 \text{ kN/m}$
$A^{\text{cs}} = 17.9^\circ\text{C}$	$\delta_{\text{max}}^{\text{tr}} = 2.95 \text{ mm}$
$A^{\text{tr}} = 21.5^\circ\text{C}$	$C = 5.7 \text{ N/m}$
$T = 25^\circ\text{C}$	

in Figure 30, they do provide a good representation of the experimental data.

#### Preisach Model Identification Using Physically Based Simplified SMA Model

The unique capability of the Preisach model to simulate any hysteretic behavior based on identification acted as a basis to identify a Preisach model from the simplified model. The main motivations behind this approach was (a) to determine the need for effective data collection for system ID-based Preisach hysteresis model and (b) to compare the differences in solving a SDOF vibration isolation system presented in Part II of this two-part paper series using the simplified model, the Preisach model identified from the experimental data and the Preisach model identified using the simplified model. The same displacement input as shown in Figure 14 is considered for identifying the Preisach model from the simplified model. The same 91 displacement data points has been considered as shown in Figure 19 and the identified model is shown in Figure 31. The response of the simplified model for the same input

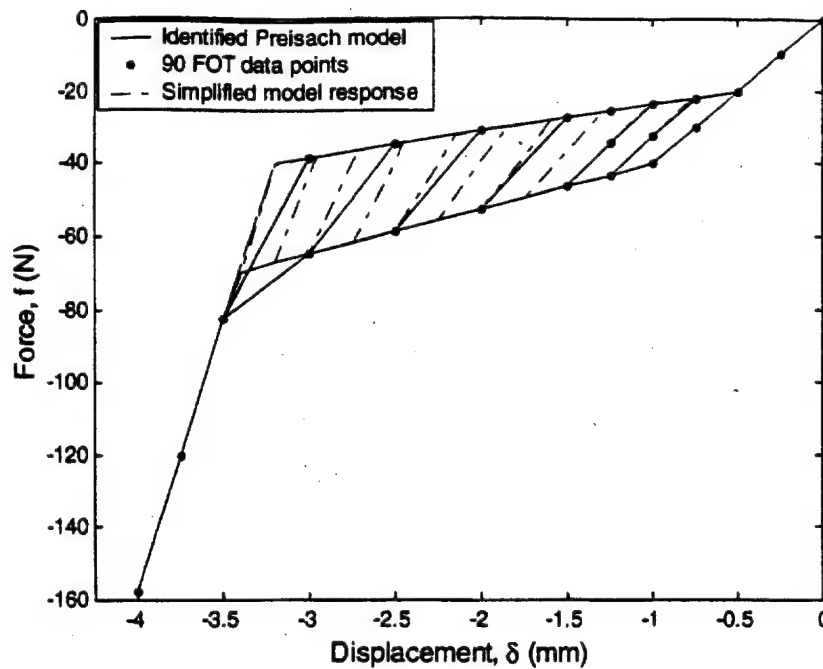


Figure 31. Comparison of Preisach model identified using simplified model and the simplified model response.

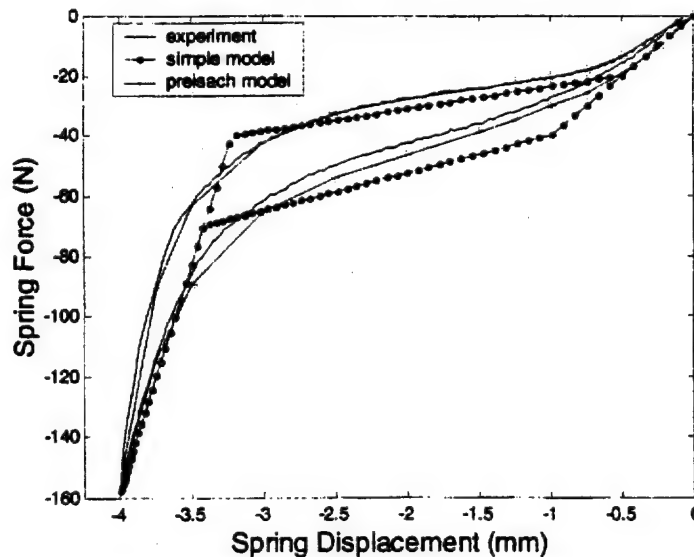


Figure 32. Comparison of calibrated models with experimental response of a SMA tube in the vibration isolation device.

is also shown in Figure 31. Note that the data points chosen for the experimental identification are not sufficient to capture the response of the simplified model. The difficulty in capturing the response of the simplified model is due to the sudden change in the force-displacement response corresponding to beginning and ending of phase transformation. This requires either additional data points or selecting different data points than the initial ones. This amplifies the need for proper data point selection for the Preisach model apart from the accuracy and computational efficiency consideration mentioned in "Preisach Model Adaptation for Pseudoelastic SMA Tube (spring) Response". Since this

identification was done just to verify the simulation results presented in Part II and not to use the Preisach model identified from the simplified model as the model for simulations, hence no modifications were done.

#### Model Comparisons

Figure 32 shows the comparison of the Preisach model and the simplified model with the actual tube response. It can be seen from Figure 32 that the Preisach model can accurately simulate the response of SMA tubes compared to the simplified SMA model. The simplified model relies on specific transformation points

for denoting beginning and ending of phase transformation whereas the Preisach model can easily depict the gradual phase transformation. Hence, this makes the Preisach model ideal for simulating an actual system consisting of nonlinear hysteretic components without sacrificing computational efficiency. However, the Preisach model is limited by the need for repeated identifications in the case of any changes in the structural response of such SMA components and has no physical correlation with SMA constitutive parameters. The need for repeated identification can be remedied by using adaptive Preisach models; however this would lead to decrease in computational efficiency. On the other hand the simplified model, since it is physically based can easily account for changes in the structural response of SMA components and is ideal for performing qualitative parametric studies by varying the phase transformation points and changing the structural stiffness, hysteresis width, operating temperature, and transformation displacement.

## CONCLUSIONS

In Part I of this work, a physically based simplified SMA model suitable for SMA-based smart structures has been presented, where the structural response is predominantly influenced by SMAs. The simplified SMA model is computationally less intensive, can be calibrated very easily from simple physical tests. Hence it can be used for preliminary design and analysis of complex SMA-based smart structures. Drawbacks of the simplified model are that it does not capture the gradual phase transformation of the structure and the effects of latent heat can only be accounted by explicitly choosing different slopes and phase transformation points for the piece-wise linear simplified SMA model. Whereas, in coupled thermomechanical models the latent heat is accounted by an appropriate energy balance equation directly coupled with the constitutive response.

A Preisach model for force-displacement response of pseudoelastic SMA tubes has also been presented in Part I of this work. The classical Preisach operator was modified for this study to minimize the implementation effort. The adopted identification implementation method helped in mitigating noise amplification in the experimental identification data and simplified the implementation of the Preisach model. The methodology followed made the Preisach model an efficient, useful, and an accurate tool for simulating the dynamic system motivated from the prototype device consisting of SMA tubes. The need for effective identification using the Preisach model has also been emphasized by performing an identification using the simplified SMA model. It has been shown that the Preisach model can

accurately simulate the response of SMA tubes compared to the simplified SMA model.

Part II of this two-part paper will discuss the effect of the hysteresis and change in stiffness on a SMA-based dynamic system by presenting numerical simulations of a generic pseudoelastic SMA spring mass system followed by simulations of the system based on the prototype device utilizing the models presented here. Detailed description of this device along with actual experimental results will also be presented in Part II followed by experimental correlations of model predictions with the actual dynamical tests and concluding remarks for the two-part paper series.

## ACKNOWLEDGMENT

The authors would like to acknowledge the financial support from the Air Force Office of Scientific Research, Grant No. F49620-01-1-0196 and the U.S. Air Force - Kirtland AFB, PO No. 00-04-6837 under the administration of Syndetix, Inc.

## APPENDIX A

### Correlation of Physically Based Simplified SMA Model with Mechanism-based Hysteretic Nonlinear Response

The major loop SMA pseudoelastic response shown in Figure 25 can also be approximated by using linear springs and slip or frictional elements. A schematic shown in Figure 33 represents one such representation of SMA pseudoelastic response using linear springs and slip or frictional elements for loading ( $L$ ) and unloading ( $U$ ) behavior. The reader is referred to similar models with different complexity levels using linear springs and

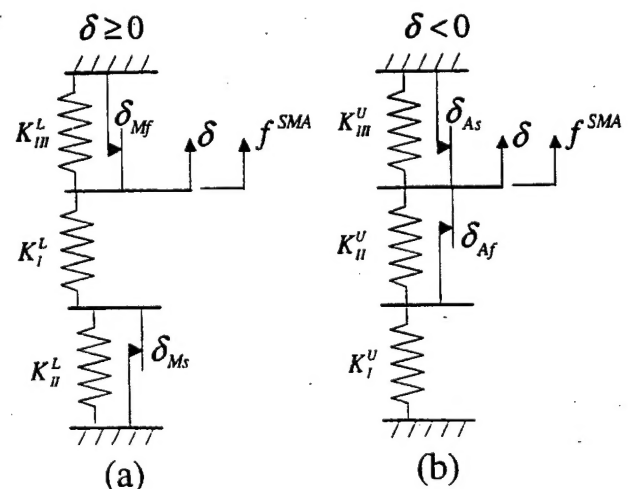


Figure 33. Representation of pseudoelastic SMA spring behavior using linear springs and slip elements during (a) loading and (b) unloading conditions.

frictional elements for modeling SMA pseudoelastic behavior in work done by Malovrh and Gandhi (2001). However, the work presented by Malovrh and Gandhi mainly deals with nonlinear hysteretic response without considering the SMA response after completion of full phase transformation.

In this section, correlations between the simplified SMA model and mechanism-based hysteretic nonlinear response is presented to show that physically based SMA models and phenomenological mechanism-based models found in the literature (Malovrh and Gandhi, 2001) can be derived from each other.

A linear spring with stiffness  $K_f^L$  shown in Figure 33(a) represents the elastic behavior of the pseudoelastic SMA spring when the SMA spring is in complete austenitic phase and undergoing loading. The corresponding governing equation expressing the relationship between force and displacement and  $K_A$  (Figure 25), is given below

$$f^{SMA} = K_A \delta \quad (40)$$

$$K_A = K_f^L \quad (41)$$

The onset of forward phase transformation (Point 1 on Figure 25) can be expressed by using a slip or a frictional element in series with a linear spring. The displacement corresponding to onset of slip is given by  $\delta_{Ms}$ . The linear strain hardening behavior during phase transformation is expressed by using a linear spring with stiffness  $K_{II}^L$  in parallel with a slip element (Figure 33(a)). The force-displacement relationship during Points 1 and 2 (see Figure 25) is given by Equation (42) and the correlation of  $K_f^L$  and  $K_{II}^L$  with  $K_{A \rightarrow M}$  (Figure 25) is given by Equation (43)

$$f^{SMA} = f_{Ms} + K_{A \rightarrow M}(\delta - \delta_{Ms}) \quad (42)$$

$$K_{A \rightarrow M} = \frac{K_f^L K_{II}^L}{K_f^L + K_{II}^L} \quad (43)$$

The end of forward phase transformation and the strain hardening behavior seen afterwards (Point 2 on Figure 25) can be represented by using a linear spring with stiffness  $K_{III}^L$  in parallel with a slip element with slip displacement  $\delta_{Mf}$ , acting against the displacement direction as shown in Figure 33. Corresponding force-displacement relationship and correlation of  $K_f^L$ ,  $K_{II}^L$ , and  $K_{III}^L$  with  $K_M$  is given by Equations (44) and (45).

$$f^{SMA} = f_{Mf} + K_M(\delta - \delta_{Mf}) \quad (44)$$

$$K_M = \frac{K_f^L K_{II}^L K_{III}^L}{K_{II}^L K_{III}^L + K_f^L K_{III}^L + K_f^L K_{II}^L} \quad (45)$$

Figure 33(b) shows the schematic for unloading conditions. The slip element with corresponding slip displacement limit of  $\delta_{Mf}$  during loading can be recalibrated to a slip displacement of  $\delta_{As}$  for unloading conditions. This corresponds to Point 3 on Figure 25 and represents start of phase transformation back into the austenitic phase. The force-displacement relationship prior to reverse phase transformation is given by Equation (46), where as, the relationship between  $K_f^U$ ,  $K_{II}^U$ , and  $K_{III}^U$  with  $K_M$  is given by Equation (47).

$$f^{SMA} = f_{As} + K_M(\delta - \delta_{As}) \quad (46)$$

$$K_M = \frac{K_f^U K_{II}^U K_{III}^U}{K_{II}^U K_{III}^U + K_f^U K_{III}^U + K_f^U K_{II}^U} \quad (47)$$

The slip element with slip displacement of  $\delta_{Ms}$  during loading can be recalibrated to a slip displacement of  $\delta_{Af}$  for unloading conditions. This corresponds to Point 4 on Figure 25 and represents end of phase transformation back into the austenitic phase. The force-displacement relationship during the reverse phase transformation is given by Equation (48), where as the relationship between  $K_f^U$  and  $K_{II}^U$  with  $K_{M \rightarrow A}$  is given by Equation (49).

$$f^{SMA} = f_{Af} + K_{M \rightarrow A}(\delta - \delta_{Af}) \quad (48)$$

$$K_{M \rightarrow A} = \frac{K_f^U K_{II}^U}{K_f^U + K_{II}^U} \quad (49)$$

After the end of reverse phase transformation the force varies linearly with displacement proportional to  $K_f^U$  and the relationship is same as shown in Equations (40) and (41).

Equations (40)–(43) represent SMA major loop response based on hysteretic nonlinear behavior using a combination of linear springs with slip elements. Following a similar approach, expressions representing minor loop response can also be derived. However, since the purpose was only to show a correlation with mechanism-based models this task has not been performed.

## NOMENCLATURE

- $\alpha$  = increasing values of displacement
- $\beta$  = decreasing values of displacement
- $\delta$  = spring displacement
- $\delta^{Af}$  = spring displacement denoting end of  $A \leftarrow M$  transformation
- $\delta^{As}$  = spring displacement denoting start of  $A \leftarrow M$  transformation
- $\delta^{Mf}$  = spring displacement denoting end of  $A \rightarrow M$  transformation

$\delta^{Ms}$  = spring displacement denoting start of  $A \rightarrow M$  transformation  
 $\delta^{tr}$  = transformation displacement  
 $\delta_{\max}$  = lower bound on displacement  
 $\delta_{\min}$  = upper bound on displacement  
 $\mu$  = weighing function in the Preisach model  
 $\sigma$  = stress  
 $A$  = austenite phase  
 $A^{0f}$  = austenite finish temperature at zero stress  
 $A^{0s}$  = austenite start temperature at zero stress  
 $f^{Af}$  = force denoting end of  $A \leftarrow M$  transformation  
 $f^{As}$  = force denoting start of  $A \leftarrow M$  transformation  
 $f^{Mf}$  = force denoting end of  $A \rightarrow M$  transformation  
 $f^{Ms}$  = force denoting start of  $A \rightarrow M$  transformation  
 $f^{SMA}$  = force exerted by SMA spring  
 $H$  = hysteresis relay operators  
 $K_A$  = stiffness of austenite phase  
 $K_M$  = stiffness of martensite phase  
 $M$  = martensite phase  
 $M^{0f}$  = martensite finish temperature at zero stress  
 $M^{0s}$  = martensite start temperature at zero stress  
 $T$  = temperature

## REFERENCES

- Abeyaratne, R. and Knowles, J.K. 1994. "Dynamics of Propagating Phase Boundaries: Thermoelastic Solids with Heat Conduction," *Archive for Rational Mechanics and Analysis*, 126(3):203-230.
- Achenbach, M. and Muller, I. 1985. "Simulation of Material Behaviour of Alloys with Shape Memory," *Arch. Mech.*, 35:537-585.
- Banks, H., Kurdila, A. and Webb, G. 1996a. "Identification of Hysteretic Control Influence Operators Representing Smart Actuators: Formulation," Tech. Rep. CRSC-TR96-14, Center for Research in Scientific Computation, North Carolina State University, Raleigh, NC.
- Banks, H., Smith, R. and Wang, Y. 1996b. *Smart Material Structures: Modeling, Estimation and Control*, John Wiley & Sons, Paris.
- Banks, H., Kurdila, A. and Webb, G. 1997. "Identification of Hysteretic Control Influence Operators Representing Smart Actuators: Convergent Approximations," Tech. Rep. CRSC-TR97-7, Center for Research in Scientific Computation, North Carolina State University, Raleigh, NC.
- Beranek, L.L. and Vör, I.L. (eds) 1992. *Noise and Vibration Control Engineering*, John Wiley and Sons, New York.
- Bernardini, D. and Vestroni, F. 2002. "Non-isothermal Oscillations of Pseudoelastic Devices," *International Journal of Non-Linear Mechanics*, Submitted for Publication.
- Bo, Z. and Lagoudas, D.C. 1999a. "Thermomechanical Modeling of Polycrystalline SMAs under Cyclic Loading, Part IV: Modeling of Minor Hysteresis Loops," *International Journal of Engineering Science*, 37:1205-1249.
- Bo, Z. and Lagoudas, D.C. 1999b. "Thermomechanical Modeling of Polycrystalline SMAs under Cyclic Loading, Part IV: Modeling of Minor Hysteresis Loops," *International Journal of Engineering Science*, 37:1174-1204.
- Brinson, L.C. 1993. "One-dimensional Constitutive Behavior of Shape Memory Alloys: Thermomechanical Derivation with Non-constant Material Functions and Redefined Martensite Internal Variable," *Journal of Intelligent Material Systems and Structures*, 4:229-242.
- Brokate, M. 1994. "Hysteresis Operators," In: Visintin, A. (ed.), *Phase Transitions and Hysteresis*, Lecture Notes in Mathematics, Vol. 1584, pp. 1-48, Springer-Verlag, Berlin, Germany.
- Collet, M., Foltete, E. and LExcellent, C. 2001. "Analysis of the Behavior of a Shape Memory Alloy Beam under Dynamic Loading," *European Journal of Mechanics and Solids*, 20:615-630.
- Feng, Z.C. and Li, D.Z. 1996. "Dynamics of a Mechanical System with a Shape Memory Alloy Bar," *Journal of Intelligent Material Systems and Structures*, 7:399-410.
- Fosdick, R. and Ketema, Y. 1998. "Shape Memory Alloys for Passive Vibration Damping," *Journal of Intelligent Systems and Structures*, 9:854-870.
- Ge, P. and Jouaneh, M. 1995. "Modeling of Hysteresis in Piezoceramic Actuators," *Precision Engineering*, 17:211-221.
- Gorbet, R.B., Morris, K.A. and Wang, D.W.L. (1997). "Stability of Control Systems for the Preisach Hysteresis Model," In: *Proc. IEEE International Conf. on Robotics and Automation*, Albuquerque, NM, Vol. 1, pp. 241-247.
- Gorbet, R.B., Wang, D.L. and Morris, K.A. 1998. "Preisach Model Identification of a Two-wire SMA Actuator," In: *Proc. IEEE International Conf. on Robotics and Automation*, Leuven, Belgium, Vol. 3, pp. 2161-2617.
- Graesser, E. and Cozzarelli, F. 1991. "Shape-memory Alloys as New Materials for Aseismic Isolation," *Journal of Engineering Materials*, 117(11), 2590-2608.
- Harris, C.M. (ed.) 1996. *Shock and Vibration Handbook*, McGraw-Hill, New York.
- HKS 1997. *ABAQUS/Standard User's Manual*, Karlsson and Sorensen, Inc., Hibbit.
- Hughes, D. 1997. "Piezoceramic and SMA Hysteresis Modeling and Compensation," Ph.D. Thesis, Rensselaer Polytechnic Institute, Troy, NY.
- Hughes, D. and Wen, J. 1994. "Preisach Modeling and Compensation for Smart Material Hysteresis," *SPIE Active Materials and Smart Structures*, 2427:50-64.
- Huo, Y.Z. 1991. "Preisach Model for the Hysteresis in Shape Memory Alloys," In: Boehler, J.P. and Khan, A.S. (eds), *Proc. Of Plasticity'91: The Third Int. Symp. on Plasticity and Its Current Applications*, Grenoble, France, Elsevier, London, pp. 552-555.
- Inman, D. 2001. *Engineering Vibration*, Prentice-Hall, Inc., Upper Saddle River, New Jersey.
- Ivshin, Y. and Pence, T.J. 1994. "A Thermomechanical Model for a One-variant Shape Memory Material," *Journal of Intelligent Material Systems and Structures*, 5:455-473.
- Khan, M.M. 2002. "Modeling of Shape Memory Alloy (SMA) Spring Elements for Passive Vibration Isolation using Simplified SMA Model and Preisach Model," Master's Thesis, Texas A & M University, College Station, TX.
- Khan, M.M. and Lagoudas, D.C. 2002. "Modeling of Shape Memory Alloy Pseudoelastic Spring Elements using Preisach Model for Passive Vibration Isolation," In: *SPIE Conference on Modeling, Signal Processing and Control in Smart Structures*, San Diego, CA.
- Krasnoselskii, A. and Pokrovskii, A. 1983. *Systems with Hysteresis*, Springer-Verlag, Heidelberg, Germany.
- Lacarbonara, W., Bernardini, D. and Vestroni, F. 2001. "Periodic and Nonperiodic Thermomechanical Responses of Shape Memory Oscillators," In: *Proc. Conf. ASME Design Engineering Technical Conference*, Pittsburgh, PA.
- Lagoudas, D. and Bhattacharyya, A. 1997. "On the Correspondence between Micromechanical Models for Isothermal Pseudoelastic Response of Shape Memory Alloys and the Preisach Model for Hysteresis," *Math. Mech. Solids*, 2(4), 405-440.
- Lagoudas, D.C. and Bo, Z. 1999. "Thermomechanical Modeling of Polycrystalline SMAs under Cyclic Loading, Part I-IV: Material Characterization and Experimental Results for a Stable Transformation Cycle," *International Journal of Engineering Science*, 37.
- Lagoudas, D.C., Bo, Z. and Qidwai, M.A. 1996. "A Unified Thermodynamic Constitutive Model for SMA and Finite Element Analysis of Active Metal Matrix Composites," *Mechanics of Composite Materials and Structures*, 3, 153-179.
- Lagoudas, D.C., Khan, M.M. and Mayes, J.J. 2001a. "Modelling of Shape Memory Alloy Springs for Passive Vibration Isolation,"

- In: *Proc. Conf. ASME International Mechanical Engineering Congress and Exposition*, New York, NY.
- Lagoudas, D.C., Khan, M.M., Mayes, J.J. and Henderson, B.K. 2002. "Parametric Study and Experimental Correlation of an SMA Based Damping and Passive Vibration Isolation Device," In: *Proc. Conf. ASME International Mechanical Engineering Congress and Exposition*, New Orleans, LA.
- Lagoudas, D.C., Mayes, J.J. and Khan, M.M. 2001b. "Simplified Shape Memory Alloy (SMA) Material Model for Vibration Isolation," In: *SPIE Conference on Modeling, Signal Processing and Control in Smart Structures*.
- Liang, C. and Rogers, C.A. 1990. "One-dimensional Thermomechanical Constitutive Relations for Shape Memory Materials," *Journal of Intelligent Material Systems and Structures*, 1:207-234.
- Malovrh, B. and Gandhi, F. 2001. "Mechanism-based Phenomenological Models for the Pseudoelastic Hysteresis Behavior of Shape Memory Alloys," *Journal of Intelligent Material Systems and Structures*, 12(1):2130.
- Mayergoys, I. 1991. *Mathematical Models of Hysteresis*, Springer-Verlag, New York.
- Mayes, J.J. and Lagoudas, D.C. 2001. "An Experimental Investigation of Shape Memory Alloy Springs for Passive Vibration Isolation," In: *Proc. Conf. AIAA Space 2001 Conference and Exposition*, Albuquerque, NM, Submitted.
- Miyazaki, S., Imai, T., Igo, Y. and Otsuka, K. 1997. "Effect of Cyclic Deformation on the Pseudoelasticity Characteristics of Ti-Ni Alloys," *Metallurgical Transactions*, 42(7):115-120.
- Ortin, J. 1992. "Preisach Modeling of Hysteresis for a Pseudoelastic Cu-Zn-Al Single-crystal," *Journal of Applied Physics*, 71(3):1454-1461.
- Otsuka, K. and Shimizu, K. 1986. "Pseudoelasticity and Shape Memory Effects in Alloys," *International Metals Review*, 31(3), 93-114.
- Otsuka, K. and Wayman, C.M. 1999. "Introduction" In: Otsuka, K. and Wayman, C.M. (eds), *Shape Memory Alloys*, Chap. 2, 27-48, Cambridge University Press, Cambridge, United Kingdom.
- Ozdemir, H. 1976. "Nonlinear Transient Dynamic Analysis of Yielding Structures." Ph.D. Thesis, University of California at Berkeley.
- Patoor, E., Eberhardt, A. and Berveiller, M. 1987. "Potentiel Pseudoélastique et plasticité de transformation martensitique dans les mono et polycristaux métalliques," *Acta Metallurgica*, 35:2779-2789.
- Preisach, F. 1935. Über die magnetische nachwirkung, *Zeitschrift für Physik*, 94:277-302.
- Qidwai, M.A. and Lagoudas, D.C. 2000. "Numerical Implementation of a Shape Memory Alloy Thermomechanical Constitutive Model using Return Mapping Algorithms," *International Journal for Numerical Methods in Engineering*, 47:1123-1168.
- Raniecki, B., Lexcellent, C. and Tanaka, K. 1992. "Thermodynamic Models of Pseudoelastic Behaviour of Shape Memory Alloys," *Arch. of Mech.*, 3.
- Seelecke, S. 2002. "Modeling the Dynamic Behavior of Shape Memory Alloys," *International Journal of Non-Linear Mechanics*, 37(8):1363-1374.
- Song, C.L., Brandon, J.A. and Featherston, C.A. 1999. "Estimation of Hysteretic Properties for Pseudoelastic Materials," In: *Proceedings of 2nd International Conference of Identification in Engineering Systems*, Swansea, Wales, pp. 210-219.
- Tanaka, K. 1986. "A Thermomechanical Sketch of Shape Memory Effect: One-dimensional Tensile Behavior," *Res Mechanica*, 18: 251-263.
- Thomson, P., Balas, G.J. and Leo, P.H. 1995. "The Use of Shape Memory Alloys for Passive Structural Damping," *Smart Materials and Structures*, 4(1):36-41.
- Visintin, A. 1994. *Differential Models of Hysteresis*, Springer-Verlag, Berlin, Germany.
- Wayman, C.M. 1983. "Phase Transformations, Nondiffusive," In: Cahn, R.W. and Haasen, P. (eds), *Physical Metallurgy*, pp. 1031-1075, North-Holland Physics Publishing, New York.
- Webb, G. 1998. "Adaptive Identification and Compensation for a Class of Hysteresis Operators," Ph.D. Thesis, Texas A & M University, College Station, TX.
- Webb, G., Kurdila, A. and Lagoudas, D. 1998. "Hysteresis Modeling of SMA Actuators for Control Applications," *Journal of Intelligent Material Systems and Structures*, 9(6):432-447.
- Yiu, Y.C. and Regelbrugge, M.E. 1995. "Shape-memory Alloy Isolators for Vibration Suppression in Space Applications," In: *Proc. 36th AIAA/ASME/ASCE/AHS/ASC Conf. Structures, Structural Dynamics, and Materials*, pp. 3390-3398. AIAA-95-1120-CP.